JOC The Journal of Organic Chemistry

pubs.acs.org/joc Article

Peptide Nucleic Acid with Double Face: Homothymine–Homocytosine Bimodal Cα-PNA (*bm*-Cα-PNA) Forms a Double Duplex of the *bm*-PNA$_2$:DNA Triplex

Manoj Kumar Gupta, Bharath Raj Madhanagopal, and Krishna N. Ganesh*

Cite This: https://dx.doi.org/10.1021/acs.joc.0c02158 Read Online

ABSTRACT: Cα-bimodal peptide nucleic acids (*bm*-Cα-PNA) are PNAs with two faces and are designed homologues of PNAs in which each aminoethylglycine (*aeg*) repeating unit in the standard PNA backbone hosts a second nucleobase at Cα through a spacer chain with a triazole linker. Such *bm*-Cα-PNA with mixed sequences can form double duplexes by simultaneous binding to two complementary DNAs, one to the base sequence on t-amide side and the other to the bases on the Cα side chain. The synthesis of *bm*-Cα-PNA with homothymine (T_7) on the t-amide face and homocytosine (C_5) on the Cα side chain through the triazole linker was achieved by solid phase synthesis with the global click reaction. In the presence of complementary DNAs dA_8 and dG_6 at neutral pH, *bm*-Cα-PNA **1** forms a higher order pentameric double duplex of a triplex composed of two *bm*-Cα-PNA-C_5:dG_5 duplexes built on a core (*bm*-Cα-PNA-T_7)$_2$:dA_8 triplex. Circular dichroism studies showed that assembly can be achieved by either triplex first and duplex later or vice versa. Isothermal titration calorimetry data indicated that the assembly is driven by favorable enthalpy. These results validate concurrent multiple complex formation by bimodal PNAs with additional nucleobases at Cα or Cγ on the *aeg*-PNA backbone and open up ways to design programmed supramolecular assemblies.

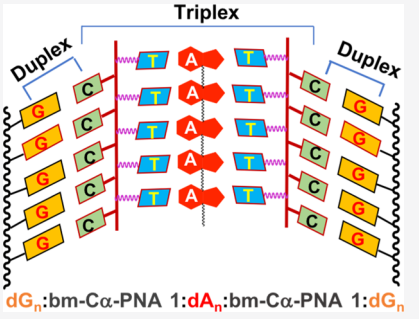

INTRODUCTION

Peptide nucleic acids (PNAs) are acyclic DNA analogues (Figure 1a) endowed with an ability to bind complementary DNA/RNA sequences to form PNA:DNA/PNA:RNA (1:1) duplexes and triplexes (PNA$_2$:DNA/RNA).[1] Complexes of PNA with DNA/RNA have specificity and affinity higher than that of analogous DNA:DNA/DNA:RNA complexes.[2] They have potential utility in nucleic acid therapeutics and proven applications as molecular probes in diagnostics.[3] Their limitations in terms of solubility and poor cell permeability have been addressed widely through various chemical modifications.[4] The chemical structure of PNA is quite simple with an achiral backbone consisting of linear aminoethyl glycine (*aeg*) units to which the nucleobases are attached through a tertiary amide bond.[1] Nevertheless, the naive structure of PNA provides ample opportunities for rational chemical modifications to influence its hybridization properties with complementary DNA/RNA/PNA in a way not obviously possible with other DNA analogues. Most substitutions confer chirality and/or cationic charges on derived backbone of PNAs.[4,5] The geometry of the *aeg* backbone in PNA ensures that the distance between the adjacent bases exactly matches the interbase dimensions on the sugar-phosphate in DNA/RNA (Figure 1b), facilitating successful, sequence-specific base pairing between the complements.[6] The adaptability of PNA backbone is attributed to its ability to preorganize its conformation for favorable binding to DNA or RNA with equal facility.[7] A controlled flexibility by restricted rotation around the tertiary amide bond favorably induces efficient and selective binding of PNA to cDNA/RNA.[2,7]

Early approaches to PNA modifications involved insertion of extra carbon into aminoethyl, glycyl, or tertiary amide segments, but these modifications produced analogues that were unsatisfactory in performance compared to that of the original *aeg* PNA.[4a] Conformationally constraining the PNA backbone through substitutions or making them cyclic showed improvements in their strength and selectivity in DNA/RNA binding.[4b−f] A large number of modifications have been carried out on nucleobases to make them functional beyond their inherent abilities to form base pairs, by conjugating them with a wide variety of ligands varying from fluorophores to metal complexes.[8] Among such modifications, the bifacial or "Janus" bases are designed as synthetic nucleobases that can recognize two natural bases from either side.[9] They are particularly useful as wedges to bridge two noncomplementary bases and have found novel applications.[10] An analogous modification is the "double-headed" DNA in which additional nucleobase was

Received: September 7, 2020

https://dx.doi.org/10.1021/acs.joc.0c02158
J. Org. Chem. XXXX, XXX, XXX−XXX

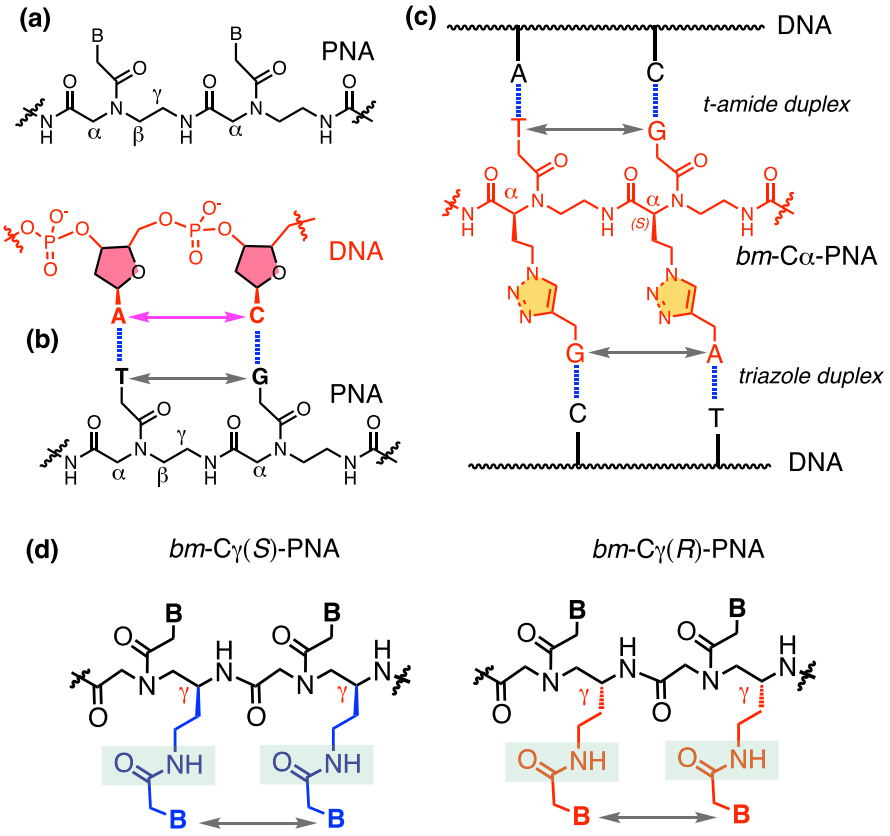

Figure 1. Structures of (a) PNA, (b) PNA/DNA duplex, (c) bimodal C*α*-PNA/DNA, and (d) bimodal C*γ*(*S*/*R*)-PNA.

linked to either at C5′ or C2′ in sugar ribose residues or at C5 of thymine, and these modifications destabilized the derived DNA/DNA duplexes.[11] However, when located near single mismatch sites, they stabilized duplexes through base pairing with mismatched base on other strand, and attempts to directly hybridize the additional conjugated bases to another complementary DNA strand were not successful.[11f] Double-headed LNA monomers incorporating second nucleobase at C2′-N of C4′−C2′-bridge lead to stabilization of duplexes, without the involvement of the additional base in any Watson−Crick (WC) pairing with base of opposite strands.[11g]

In light of the above work on bifacial PNA[9,10] and double-headed DNA analogues,[11] we have recently reported new types of PNA analogues *bimodal*-C*α*-PNA[12a] (Figure 1c) and *bimodal*-C*γ*(*S*/*R*)-PNA[12b] (Figure 1d) in which the *aeg* backbone of PNA acquires bifacial character. In these analogues, a single strand PNA can simultaneously bind two different DNA strands (Figure 1c), one from each side to form PNA/DNA double duplexes. In these PNAs, each repeating *aeg* unit on the backbone hosts an additional nucleobase (A/G/C/T) linked via an ethyltriazole sidechain at C*α* of the glycyl component (Figure 1c) or an alkylamido chain at C*γ* of the ethylenediamine component. Such "bimodal" PNAs with mixed purine/pyrimidine sequences on both t-amide and triazole sides form two PNA/DNA duplexes, hosted on a common PNA backbone.[12a] Recently, we have shown that the sidechain carrying second nucleobase can be hosted also on C*γ* in both *S* and *R* stereochemical dispositions and such C*γ*-bimodal PNAs also form double duplex, one from each face.[12b] The previously reported bimodal PNAs have mixed sequences on both faces and so form duplex. Since PNAs carrying homo purine/pyrimidine sequences are known to form PNA_2/DNA triplexes,[2] we describe here bimodal PNAs that have homothymine (T_7) sequence on t-amide face and homocytosine (C_5) on the C*α* side chain face. We demonstrate that these form double duplex of a triplex dG_6:C_5-*bm*-C*α*-PNA:dA_8:*bm*-C*α*-PNA-C_5:dG_6 (triplex component indicated in the underlined text) as a pentameric (2× *bm*-C*α*-PNA, 3× DNA) complex, in comparison to the ternary double duplex in our previous report.[12] The results demonstrate the ability of bimodal PNAs (*bm*-C*α*-PNA) to template higher order nucleic acid assemblies based on the nature of sequences.

The structures of designed targets *bm*-C*α*-PNA **1**, *bm*-C*α*-PNA **2**, and *iso*-C*α*-PNA **3** are shown in Figure 2. All have homocytosine (C_5) sequence on the C*α*-triazole side, while on t-amide face, *bm*-C*α*-PNA **1** has homothymines (T_7) and *bm*-C*α*-PNA **2** contains mixed sequence. The sequences were chosen for no particular reason other than the ease of synthesis and to demonstrate the formation of higher order assembly from double duplex to double duplex of a triplex. The T_7 sequence on *bm*-C*α*-PNA **1** can form a triplex with dA_8 at pH 7.0, while mixed sequence in *bm*-C*α*-PNA **2** can only form duplex with cDNA. The homocytosinyl C_5 can form triplex with dG_n at acidic pH, while at neutral pH, may form a parallel duplex with reverse WC or Hoogsteen (HG) base pairing.[13] The control PNA *iso*-C*α*-PNA **3** holding bases only on C*α* side chain was used to examine the independent ability of C*α*-triazole-C_5 for hybridization with dG_6. The *iso*-C*α*-PNA **4** that has G_5 on the triazole side was also synthesized to test the sequence-dependent formation of C*α*-triazole duplexes. It is demonstrated that isomeric PNA structures with nucleobases on C*α*-sidechain form duplex with complementary DNA with equal capability as the standard *aeg*-PNA. In all cases, the stereochemical disposition at C*α*-sidechain was *S* [*bm*-C*α*(*S*)-

https://dx.doi.org/10.1021/acs.joc.0c02158
J. Org. Chem. XXXX, XXX, XXX−XXX

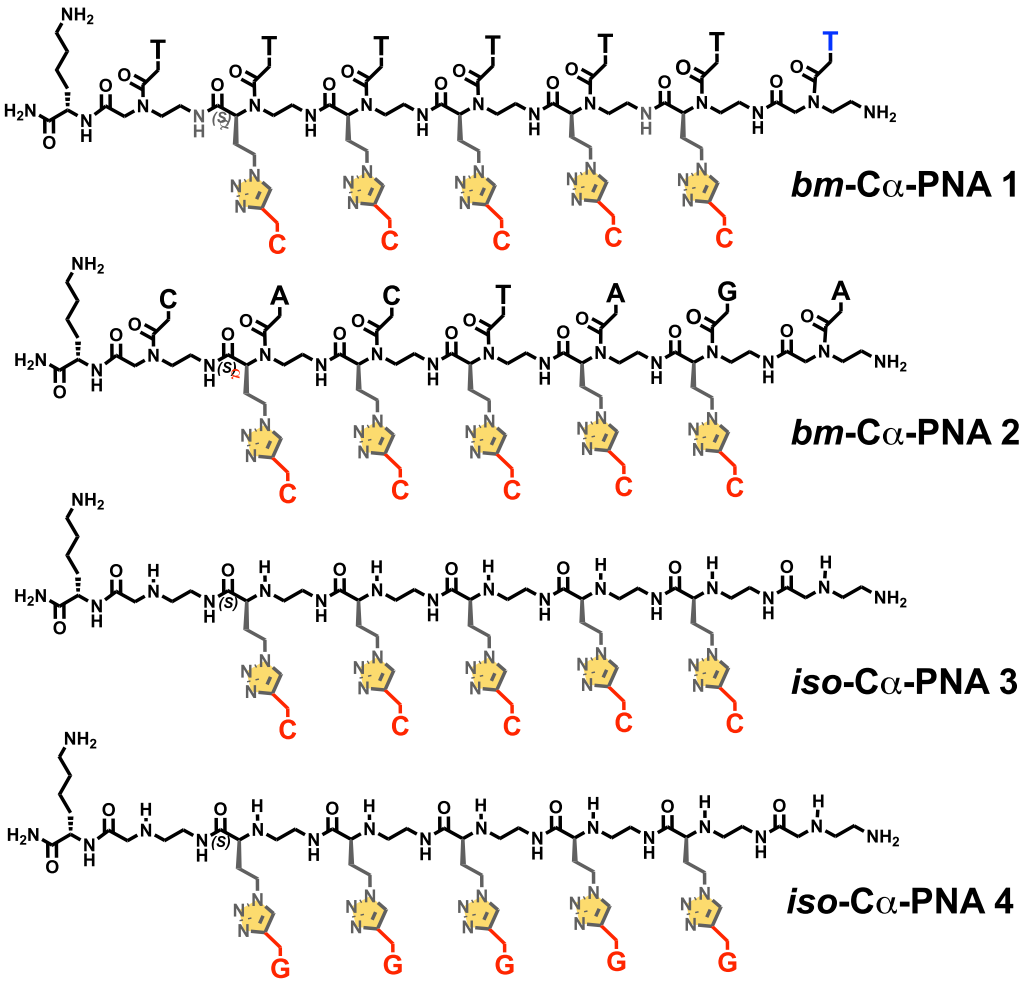

Figure 2. Chemical structures of bimodal PNA oligomers: *bm*-C*α*-PNA **1**, *bm*-C*α*-PNA **2**, *iso*-C*α*-PNA **3**, and *iso*-C*α*-PNA **4**.

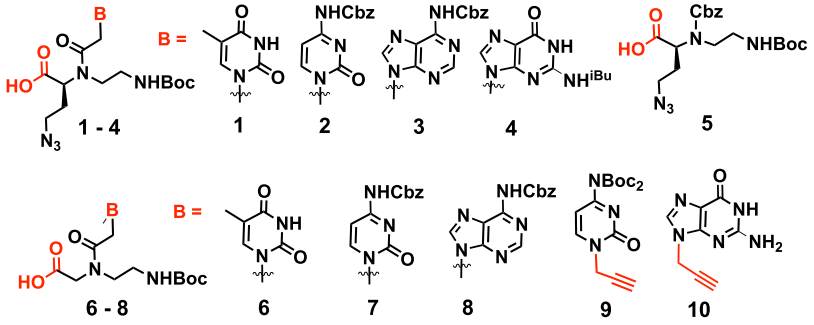

Figure 3. Structures of C*α*(*S*)-ethylazido PNA monomers (**1**−**4**), C*α*(*S*)-ethylazido-N(Cbz) monomer (**5**), *aeg* PNA (T/C/A) monomers (**6**−**8**), N1-propynyl-C (**9**), and N9-propynyl-G (**10**).

PNA and *iso*-C*α*(*S*)-PNA] that can be prepared easily from L-glutamine although it is known in general that the C*α*(*R*)-substitutions gave a higher stability of PNA/DNA hybrids.[14]

RESULTS AND DISCUSSION

The various C*α*-ethylazido monomers **1**−**5** required for the solid phase assembly of corresponding PNA oligomers are shown in Figure 3. These were synthesized by following procedures previously reported by us (see the Supporting Information in ref 12a), and the standard PNA monomers **6**−**8** were obtained from the commercial source. N1-propynyl C (**9**) and N9-propynyl G (**10**) were synthesized, according to the known literature procedures.[15] The PNA oligomers obtained after solid phase synthesis carried the ethylazido sidechain at C*α* for a one-step click reaction with propynes **9** or **10** on resin to obtain the desired final bimodal *bm*-C*α*-PNA **1**, *bm*-C*α*-PNA **2** and the *iso*-PNA oligomers, *iso*-C*α*-PNA **3** and *iso*-C*α*-PNA **4**.

Solid Phase Synthesis of Bimodal-C*α*-PNA and *iso*-C*α*-PNA Oligomers. The C*α*-substituted bimodal PNA oligomers (Figure 2) were synthesized by solid phase synthesis (Schemes 1 and 2) using L-lysine-derivatized 4-Methylbenzhydrylamine (MBHA) resin employing standard protocols of Boc chemistry.[16] For *bm*-C*α*-PNA **1** (Scheme 1), the initial Boc

https://dx.doi.org/10.1021/acs.joc.0c02158
J. Org. Chem. XXXX, XXX, XXX−XXX

Scheme 1. Solid Phase Synthesis of *bm*-Cα-PNA 1

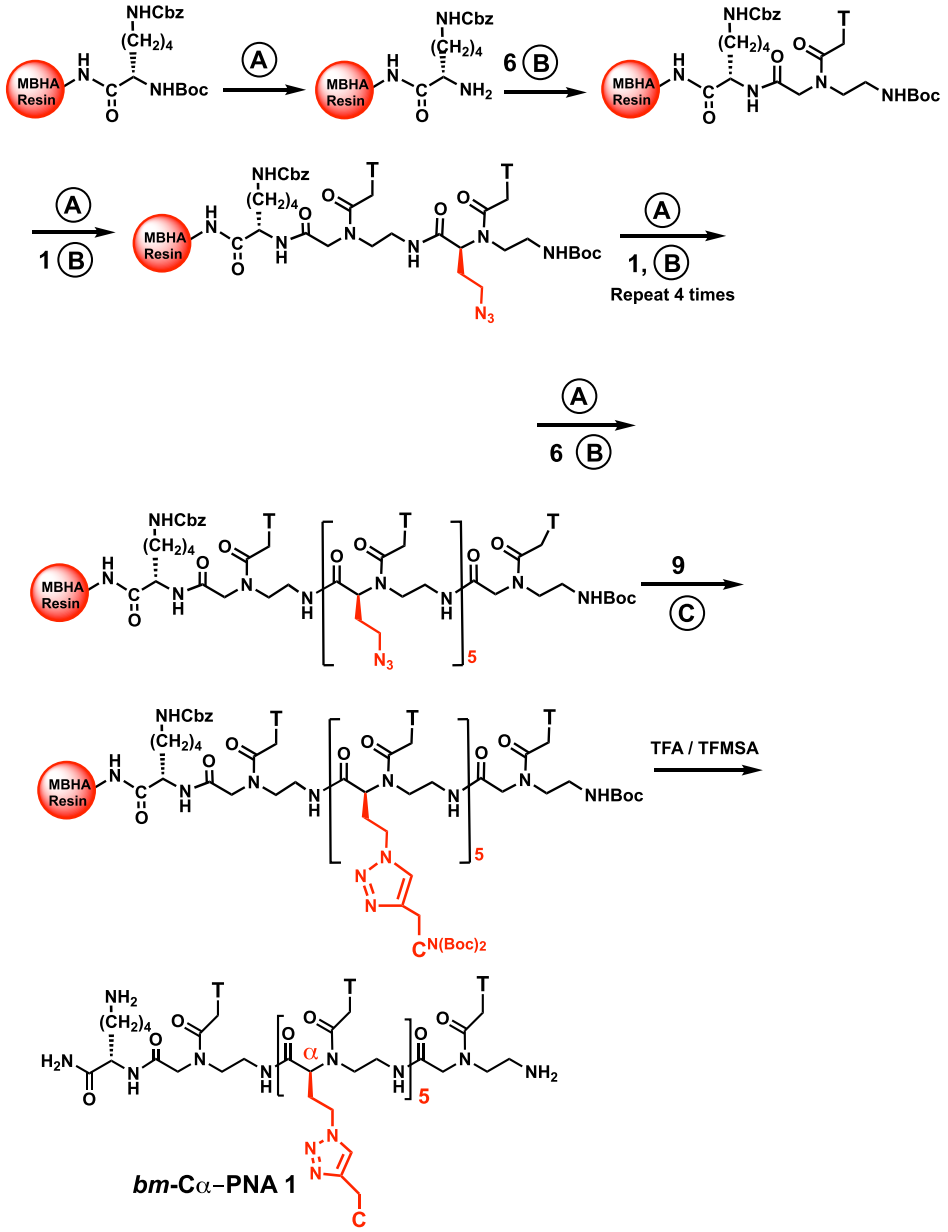

deprotection (step A) on resin was followed by first coupling with *aeg*-PNA T monomer **6**. Subsequently, each cycle consisted of (i) N-Boc deprotection with trifluoroacetic acid (TFA) and neutralization with *N*,*N*-diisopropylethylamine (DIPEA) to get free NH_2 on resin (step A) and (ii) coupling with PNA monomer acid **1** in the presence of coupling agents (step B). The cycle was repeated five times, and last coupling was carried out with *aeg*-PNA T monomer **6**. After completing the cycles, the resin bound oligomer was subjected to a global click reaction with N1-propynyl cytosine **9**, to yield *bm*-Cα-PNA **1** oligomer residing on the resin. The *bm*-Cα-PNA **2** having mixed sequence on t-amide side and C_5 on triazole side was synthesized by the solid phase protocol (Scheme 2), with the first coupling of L-lysine-derivatized MBHA using *aeg*-PNA C monomer **7** followed by step A and coupling with Cα-azido monomer A (**3**). Subsequent sequential deprotection and coupling with appropriate monomers **1**−**4** were followed by final coupling with *aeg*-PNA A monomer **8**. The assembled PNA oligomers (Schemes 1 and 2) were subjected to a single-step click reaction[12a] with N1-propyne C (**9**) to install the triazole side pentameric C_5 sequence. Employing a similar solid phase synthesis protocol using monomer **5**, followed by a one-step click reaction with N1-propyne C (**9**) or N1-propyne G (**10**)[15] gave *iso*-Cα-PNA **3** and *iso*-Cα-PNA **4** having nucleobases C_5 and G_5 on triazole side, respectively (Supporting Information, S7). The highlight of the solid phase synthesis of bimodal PNAs described here is the use of a global click reaction to install all nucleobases in a single step, thus avoiding synthesis of bimodal PNA monomers having different combinations of bases on t-amide and triazole side. Use of propynes of T and A should allow synthesis of triazole face bimodal PNAs containing homo-oligomeric T and A bases. The reagent and reaction conditions to achieve the global click reaction were optimized to achieve complete reactions of all Cα-azido sidechains in a single step by monitoring the resin-cleaved product by phase reverse high-

https://dx.doi.org/10.1021/acs.joc.0c02158
J. Org. Chem. XXXX, XXX, XXX−XXX

Scheme 2. Solid Phase Synthesis of *bm*-C*α*-PNA 2

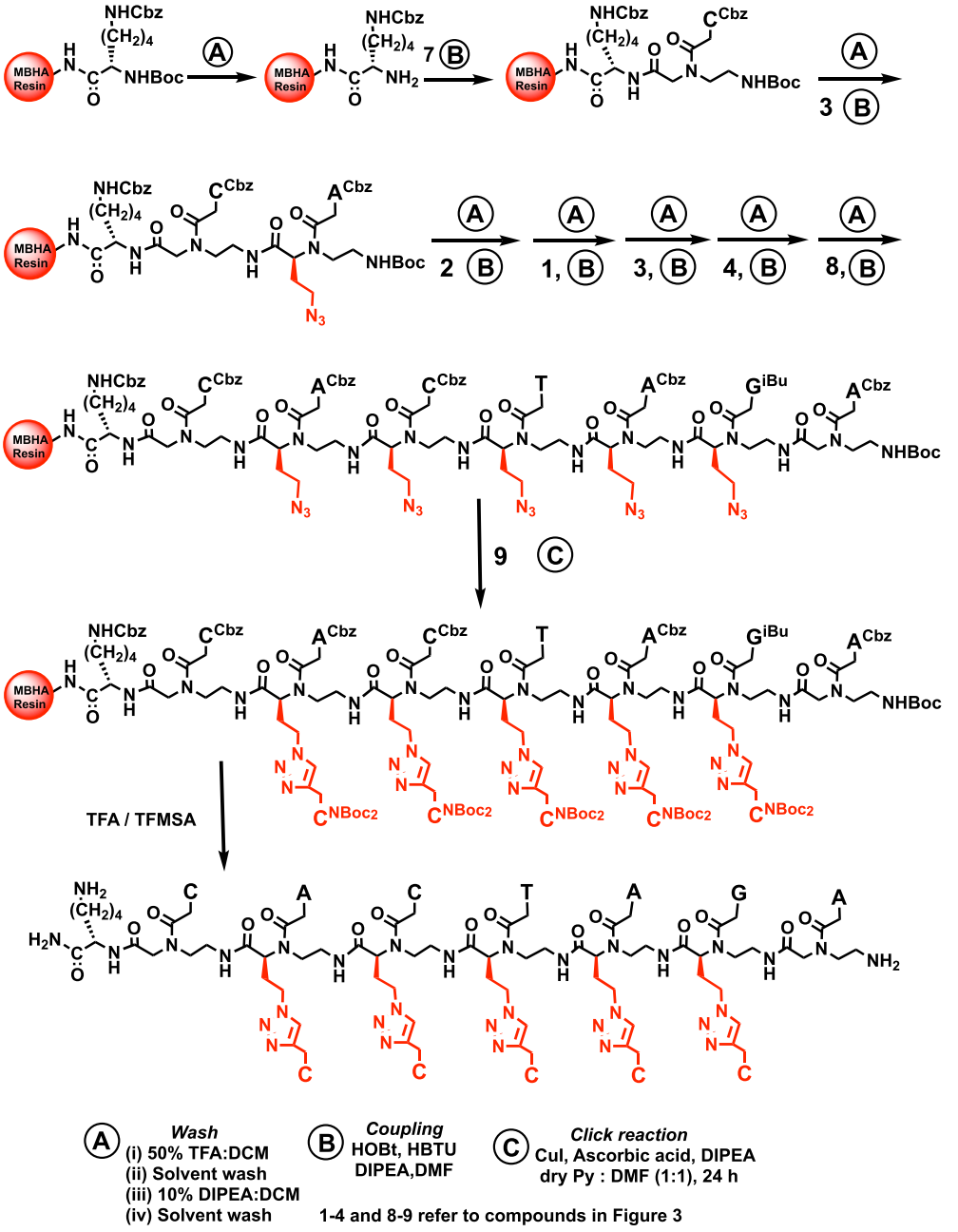

performance liquid chromatography (HPLC) and mass spectral data.

After the on-resin synthesis, the bimodal and *iso*-PNA oligomers were cleaved from the solid support MBHA resin using TFA/trifluoromethanesulfonic acid (TFMSA) which also deprotected the bases. This resulted in PNA oligomers *bm*-C*α*-PNA **1**, *bm*-C*α*-PNA **2**, and *iso*-C*α*-PNA **3** having L-lysine amide at C-termini. The product PNA oligomers were purified by semipreparative reverse phase HPLC, rechecked for purity by analytical HPLC, and characterized by high-resolution matrix-assisted laser desorption ionization time-of-flight (MALDI-TOF) mass spectral measurements (Table 1).

Biophysical Studies on PNA/DNA Complexation. The bimodal PNAs *bm*-C*α*-PNA **1**, *bm*-C*α*-PNA **2**, and *iso*-C*α*-PNA **3** were individually hybridized with DNA sequences complementary to triazole side (dG_6, DNA **1**) and t-amide side (dA_8, DNA **2**). While PNA-T_n sequences are known to form PNA_2/DNA triplex with dA_n at neutral pH, PNA-C_n/PNA-G_n sequences form corresponding PNA_2/DNA triplexes with dG_n/dC_n only at acidic pH, due to the requirement of C-protonation. At neutral pH, the predominant complex is PNA/DNA (1:1) duplex and such duplexes are preferred in parallel

Table 1. MALDI-TOF Spectral Data for *bm*-C*α*-PNA and *iso*-C*α*-PNA Oligomers

entry	oligomer	mol. formula	calc. mass	obs. mass
1	*bm*-C*α*-PNA **1**	$C_{128}H_{163}N_{61}O_{34}$	3100.10 $[M]^+$	3100.60
2	*bm*-C*α*-PNA **2**	$C_{128}H_{129}N_{75}O_{26}$	3185.33 $[M + Na]^+$	3185.48
3	*iso*-C*α*-PNA **3**	$C_{79}H_{121}N_{47}O_{13}$	1937.15 $[M]^+$	1937.49
4	*iso*-C*α*-PNA **4**	$C_{84}H_{123}N_{57}O_{13}$	2138.28 $[M + H]^+$	2138.20

https://dx.doi.org/10.1021/acs.joc.0c02158
J. Org. Chem. XXXX, XXX, XXX−XXX

orientation and with HG or reverse WC base pairing.[13,17] The binding stoichiometry of *bm*-Cα-PNA **1**:dG$_6$ (DNA **1**) complexation was determined by the Job plot.[18] This involved mixing of both components at pH 7.0 with continuous varying ratios keeping the total concentration constant (5 μM) and following changes in the ratio of UV absorbance (260/290 nm) (Figure 4). The break point in the plot indicated the

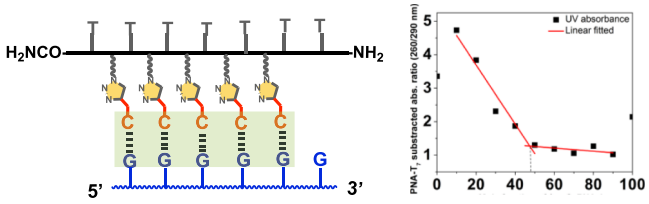

Figure 4. Continuous variation Job plot of *bm*-Cα-PNA **1**:DNA **1** duplex.

binding stoichiometry to be 1:1 for the *bm*-Cα-PNA **1**:dG$_6$ complex, suggesting it to be a duplex from triazole face. This ruled out higher order tetraplexes from self-assembly of either *bm*-Cα-PNA **1** or dG$_6$ under the experimental conditions of measurements.

Thermal Stability of Bimodal and *iso*-Cα-PNA Triazole Duplexes with dG$_6$. The successful formation of triazole face duplexes of bimodal PNAs *bm*-Cα-PNA **1**, *bm*-Cα-PNA **2**, *iso*-Cα-PNA **3**, and *iso*-Cα-PNA **4** were shown by temperature-dependent UV absorbance at 260 nm. Observation of sigmoidal transitions in UV−*T* plots and single peak in first derivative curves confirmed the formation of the duplexes with T_m corresponding to midpoint of transition.[19] The individual PNA/DNA complexes were constituted by mixing equimolar amounts of PNAs with complementary DNA **1** (dG$_6$) in buffer followed by annealing. Figure 5 shows UV−*T* plots of *bm*-Cα-PNA **1**, *bm*-Cα-PNA **2**, and *iso*-Cα-PNA **3** triazole duplexes with dG$_6$ and *iso*-Cα-PNA **4** duplex with complementary dC$_6$. All duplexes exhibited single sigmoidal transition for their triazole duplexes confirmed by their derivative plots, and T_ms obtained from the mid-point of corresponding transitions are shown in individual UV−*T* plots of duplexes (Figure 5). The bimodal duplexes *bm*-Cα-PNA **1**:dG$_6$ (**5B**) and *bm*-Cα-PNA **2**:dG$_6$ (**5C**) duplexes had T_ms 50.7 and 51.2 °C, respectively, while the *iso*-Cα-PNA **3**:dG$_6$ duplex (**5A**) had a lower T_m of 40.3 °C. The *iso*-Cα-PNA **4**:dC$_6$ duplex (**5D**) with G$_6$ on PNA backbones and C$_6$ on DNA had the highest T_m (63.9 °C) among the triazole duplexes. These results demonstrated successful formation of triazole duplexes from the new isomorphic and bimodal PNA backbones having nucleobases on Cα-sidechain on the *aeg* backbone, which is a new observation in the PNA field. The *bm*-Cα-PNA:DNA duplexes (**5B**) with homothymines on t-amide face had higher T_m (+10.4 °C) than analogous *iso*-Cα-PNA:DNA duplex (**5A**), suggesting the influence of attached t-amide linked T$_7$ nucleobases in stabilizing the triazole side duplex. Among the two *iso*-Cα-PNA triazole duplexes, the duplex from *iso*-Cα-PNA **4** with G$_5$ on PNA backbone (**5D**) has a higher stability (+24 °C) than the duplex from *iso*-Cα-PNA **1** with C$_5$ on PNA backbone (**5A**). All C$_5$:G$_5$ PNA:DNA duplexes are shown in antiparallel orientation that are generally more stable,[6b] but parallel orientation cannot be ruled out.

The T$_7$ sequence on t-amide side in bimodal PNA *bm*-Cα-PNA **1** also formed complex with complementary dA$_8$ (DNA **2**) as observed from single transition at T_m 30.3 °C (Figure 6A). It was identified as the triplex (*bm*-Cα-PNA **1**)$_2$:dA$_8$ based on its characteristic circular dichroism (CD) profile (see later). This is consistent with the literature precedence that PNA-T$_n$ with complementary dA$_n$ predominantly forms PNA$_2$:DNA triplex at neutral pH (7.0) with the PNA strand that binds by HG H-bonding is in parallel orientation.[6,20] The *bm*-Cα-PNA **2** that has mixed sequence on t-amide side forms antiparallel duplex with DNA **3** and showed a slightly higher T_m (39.5 °C), perhaps due to the presence of G in the sequence (Figure 6B). Thus, while homo oligomeric C$_5$ on Cα-sidechain in *bm*-Cα-PNA **1**, *bm*-Cα-PNA **2**, and *iso*-Cα-PNA **3** form PNA/DNA (1:1) duplexes, the t-amide linked homo-oligomeric T$_7$ forms (PNA)$_2$/DNA (2:1) triplex. It is

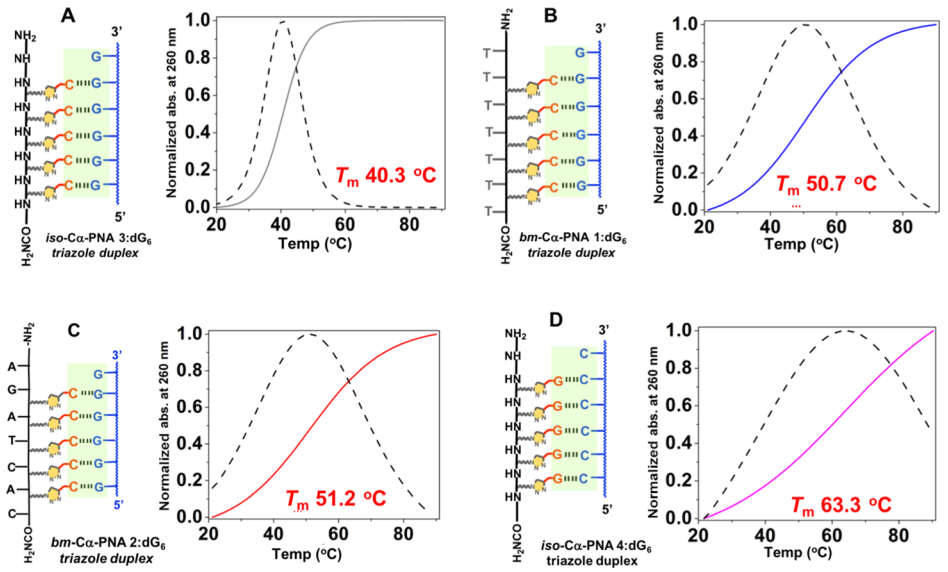

Figure 5. Triazole (A−D) duplexes of *iso*-Cα-PNA **3** (A), *bm*-Cα-PNA **1** (B) and *bm*-Cα-PNA **2** (C) with dG$_6$ (D) *iso*-Cα-PNA **4** with dC$_6$. The UV−*T* plots (continuous line sigmoidal and broken line first derivative curve) of triazole duplexes (A−D) are shown on the right side. The T_m of each complex is indicated in the red text. The individual complexes indicated in figure are referred to as 5A, 5B, 5C, and 5D throughout the text.

https://dx.doi.org/10.1021/acs.joc.0c02158
J. Org. Chem. XXXX, XXX, XXX−XXX

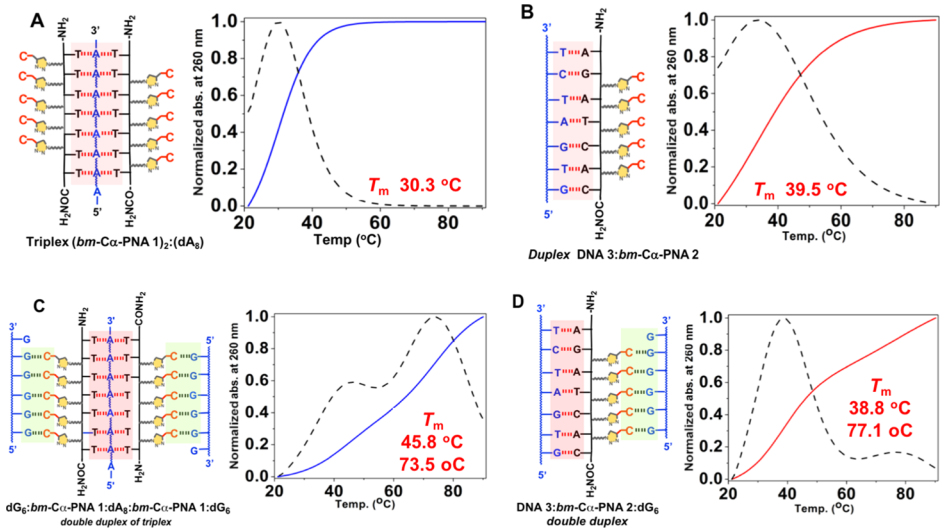

Figure 6. Complexes and UV−T plots of (A) t-amide face triplex (*bm*-Cα-PNA **1**)$_2$:(dA$_8$), (B) t-amide face duplex *bm*-Cα-PNA **2** with DNA **3**, (C) pentameric (double duplex of triplex) complex of *bm*-Cα-PNA **1** with dA$_8$ (triplex) dG$_6$ (duplexes), and (D) ternary double duplex of *bm*-Cα-PNA **2** with DNA **3** and dG$_6$. On right side, corresponding UV−T plots with the first derivative curves superimposed on sigmoidal melting transitions. T_ms are indicated in the red text. The individual complexes indicated in figure are referred to as **6A**, **6B**, **6C**, and **6D** throughout the text.

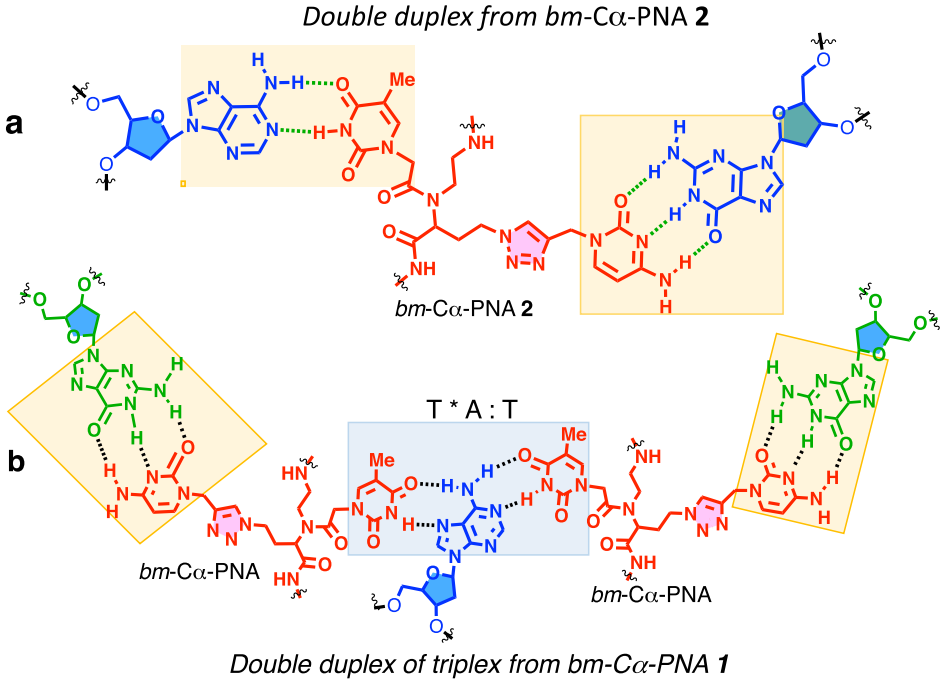

Figure 7. Formation of base pairs in (a) bimodal double duplex and (b) double duplex of triplex. Green and blue rings represent DNA.

interesting to note that in spite of lesser number of nucleobases on triazole side, the T_m of triazole duplexes were higher than that of t-amide triplex/duplex. In the case of *iso*-Cα-PNAs, this could be due to the presence of cationic secondary amine groups on the backbone, partially contributing to the stability of duplexes through electrostatic interactions with anionic DNA backbone.

After establishing that bimodal PNAs *bm*-Cα-PNA **1** and *bm*-Cα-PNA **2** form hybrids (duplex/triplex) individually from both triazole and t-amide side, simultaneous formation of hybrids from both sides was examined. This was carried out by mixing the individual bimodal PNAs with equimolar amounts of appropriate DNAs complementary to both faces followed by annealing. The UV−T plot of such a constituted complex from *bm*-Cα-PNA **1** with dA$_8$ and dG$_6$ showed two successive well-resolved transitions (double sigmoidal curves) at T_{m1} (45.8 °C) and T_{m2} (73.5 °C) (Figure 6C). Both T_ms are higher than the transitions seen in isolated complexes (**5B** and **6A**), suggesting simultaneous formation of hybrids from both t-amide and triazole sides. Since T$_7$ on t-amide side of *bm*-Cα-PNA **1** forms triplex with dA$_8$ (Figure 6A) and duplex on Cα-triazole side in the presence of dG$_6$ (Figure 5B), the composite pentameric complex should correspond to double duplex of a triplex dG$_6$:*bm*-Cα-PNA **1**:dA$_8$:*bm*-Cα-PNA **1**:dG$_6$ (Figure 6C).

The bimodal *bm*-Cα-PNA **2** that has mixed sequence on t-amide side cannot form triplex, and the resultant ternary complex in the presence of DNA **3** and dG$_6$ is a double duplex

https://dx.doi.org/10.1021/acs.joc.0c02158
J. Org. Chem. XXXX, XXX, XXX−XXX

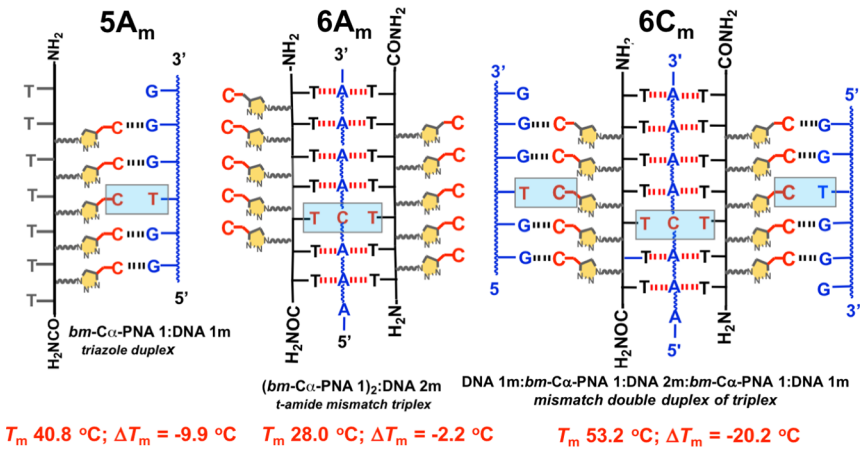

Figure 8. Mismatched complexes of *bm*-Cα-PNA **1** with DNA **1m**, DNA **2m**, and DNA **1m** + DNA **2m** buffer: 10 mM sodium cacodylate, pH 7.2, NaCl 10 mM, concentration of each strand was 3 μM.

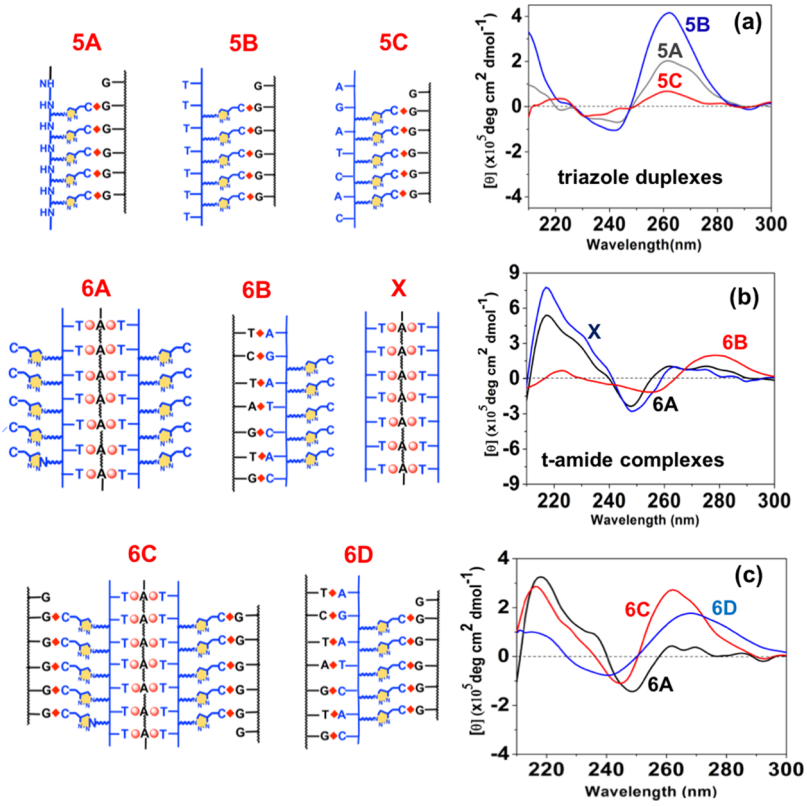

Figure 9. CD spectra at 10 °C of triazole and t-amide *bm*-Cα-PNA:DNA complexes: (a) triazole duplexes. **5A** *iso*-Cα-PNA **3**:dG$_6$, **5B** *bm*-Cα-PNA **1**:dG$_6$, and **5C** *bm*-Cα-PNA **2**:dG$_6$; (b) t-amide complexes. **6A** (*bm*-Cα-PNA **1**)$_2$:dA$_8$ triplex, **6B** DNA **3**:*bm*-Cα-PNA **2**, t-amide duplex and **X**, (PNA-T$_7$)$_2$:dA$_8$ triplex, (c) **6C** dG$_6$:*bm*-Cα-PNA **1**:dA$_8$:*bm*-Cα-PNA **1**:dG$_6$, double duplex of triplex and **6D**, DNA **3**:*bm*-Cα-PNA **2**:dG$_6$, and double duplex. Buffer, 10 mM sodium cacodylate, pH 7.2, NaCl 10 mM.

(Figure 6D). The melting curve indicated two sigmoidal transitions, similar to the pattern seen earlier in mixed sequence double duplexes.[12] The two T_ms of 38.8 and 77.1 °C were well resolved in the derivative plots with ΔT_m of 38.3 °C in the *bm*-Cα-PNA **2** ternary complex. The first transition was of a higher amplitude and relatively sharper as compared to the second weak and broader transition. Although bimodal PNAs were designed to form double duplexes, the synergistic effect on stabilization of two duplexes coexisting on a single PNA backbone is an interesting outcome. The individual base pairing schemes possible in double duplexes and double duplex of triplex are shown in Figure 7.

Mismatch *bm*-Cα-PNA 1:DNA Complexes. In order to validate the sequence specificity of triplex and duplex formation in *bm*-Cα-PNA **1** complexes, UV-melting studies were carried out with hybrids constituted from DNA **1m** (5′-GGTGGG-3′) and DNA **2m** (5′-AAACAAAA-3′) that carry single C:T base mismatches (Figure 8). The mismatched duplexes exhibited single sigmoidal transition (Supporting Information, Figure S14) but with lesser T_m compared to perfect duplexes. The T_m of triazole duplex *bm*-Cα-PNA

https://dx.doi.org/10.1021/acs.joc.0c02158
J. Org. Chem. XXXX, XXX, XXX−XXX

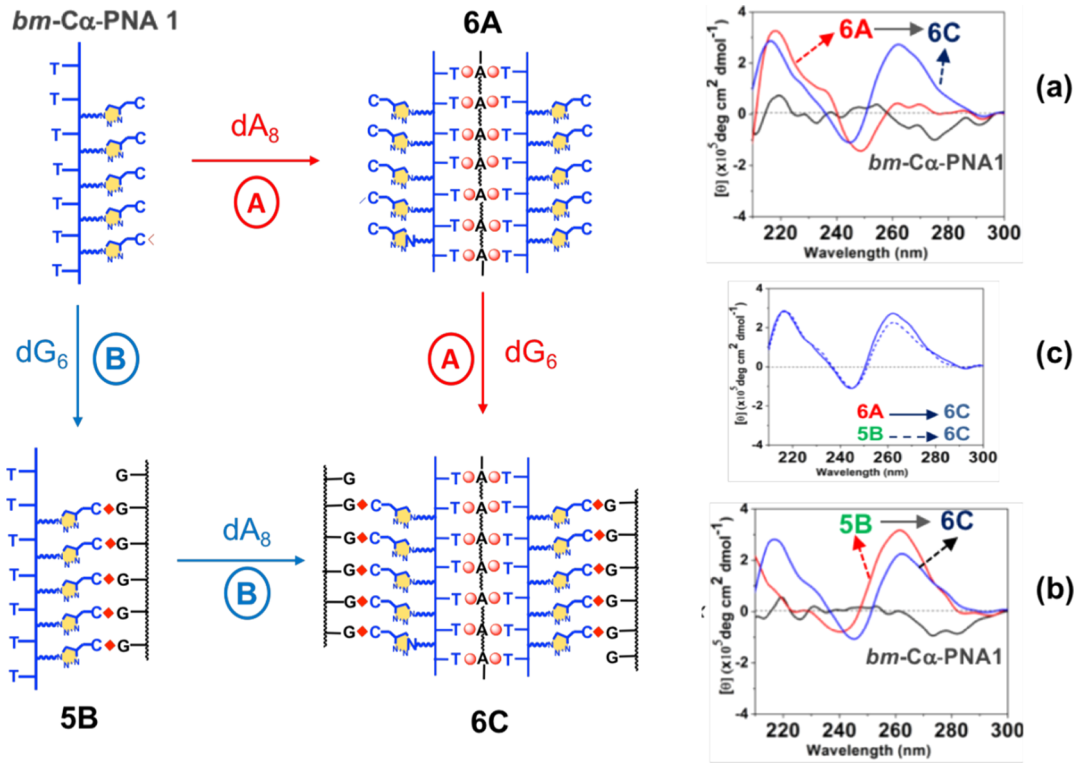

Figure 10. Two pathways A and B lead to the same final double duplex of triplex from *bm*-C*α*-PNA **1**. **5B**, **6A**, **6C** refer to complexes shown in Figures 5 and 6. (a,b) CD spectra of sequential additions of dA_8 (path A) and dG_6 (path B), respectively, and (c) overlapping CD spectra of triplex of duplex generated by two different pathways.

1:DNA **1m** with single mismatch (Figure 8, $\mathbf{5A_m}$) was 40.8 °C and was lowered by 9.9 °C compared to that of perfect duplex (*bm*-C*α*-PNA **1**:DNA **1**). The T_m of t-amide face triplex (*bm*-C*α*-PNA **1**)$_2$:DNA **2m** having mismatched triad T:C:T (Figure 8, $\mathbf{6A_m}$) was 28.0 °C, lowered by 2.2 °C for the perfect triplex (*bm*-C*α*-PNA **1**)$_2$:dA_8. In comparison, the pentameric complex DNA **1m**:*bm*-C*α*-PNA **1**:DNA **2m**:*bm*-C*α*-PNA **1**:DNA **1m** with three mismatches (Figure 8, $\mathbf{6C_m}$) gave a single transition with T_m = 53.2 °C (lower by 20.2 °C compared to perfect duplex). Unlike the two well-resolved transitions seen in perfect complex **6C**, the single transition in mismatch complex $\mathbf{6C_m}$ suggested that the three constituent strands (*bm*-C*α*-PNA **1**, DNA **1m**, and DNA **2m**) dissociate in a single step. A similar situation was seen in the lower stability of duplexes of *bm*-C*α*-PNA **2** with mismatched DNA **3m** and DNA **4m** that carry two mismatches per duplex (Supporting Information, S15). Notably, the T_m of the mismatched complex was higher than that of constituent duplex and triplex, indicating that the mutual stabilizing influence found in bimodal PNA/DNA hybrids over constituent individual triplex and duplex holds good even in mismatched complexes. Overall, these results provided further evidence for two important attributes of bimodal PNAs: (i) the complex formation is sequence specific and (ii) synergistic stabilizing effects in the simultaneous formation of triplex and duplex from amide and triazole sides.

CD Spectra of Bimodal PNA/DNA Complexes. The identity of duplexes and triplexes formed by *bm*-C*α*-PNA was examined by their CD spectral profiles. The CD spectra of the bimodal PNA triazole complexes are shown in Figure 9. The *iso*-C*α*-PNA **3**:dG_6 duplex (**5A**) showed a positive band around 260 nm and a weaker negative band around 240 nm with crossover at 247 nm. The homooligomeric *bm*-C*α*-PNA **1**:dG_6 (**5B**) duplex also showed a similar profile (Figure 9a, trace **5B**) but with much stronger intensity band at 260 nm. The mixed sequence bimodal PNA *bm*-C*α*-PNA **2** (**5C**) had a lower intensity positive band at 260 nm, accompanied by a minor band at 230 nm and a positive tail beyond 220 nm (Figure 9a, trace 5**C**). The overall CD profiles of the three duplexes were similar to the CD spectra of the corresponding duplexes from *aeg*-PNA (PNA-C_5:dG_6) and DNA/DNA (dC_6:dG_6) (Supporting Information, Figure S16) and typical of PNA/DNA duplexes.[21] The formation of duplex by *bm*-C*α*-PNA **1**:dG_6 (**5B**) was also confirmed by Job's plot, which showed 1:1 stoichiometry for this duplex (Figure 4). These results clearly confirm the formation of *iso*-C*α*-PNA and *bm*-C*α*-PNA duplexes.

The CD spectra of t-amide complex *bm*-C*α*-PNA **1**:dA_8 **6A** exhibited a major positive band at 220 nm (shoulder at 228 nm), low intensity positive bands at 262 nm and 282 nm, accompanied by a moderate negative band at 250 nm (Figure 9b, trace **6A**). These are the characteristics of the (PNA-T_7)$_2$:dA_8 triplex (shown in Figure 9b, trace **X**), which identified the formation of (*bm*-C*α*-PNA **1**)$_2$:DNA **2** triplex **6A**. This triplex shows a single transition in the UV−*T* plot (Figure 6A) as expected for PNA_2/DNA triplex.[21] In comparison, *bm*-C*α*-PNA **2** **6B** with the mixed sequence on t-amide face cannot form a triplex and binds complementary DNA **3** to form t-amide duplex DNA **3**:*bm*-C*α*-PNA **2** and shows a CD profile (Figure 9b, trace **6B**) typical of duplexes but with a slight shift of positive band.

In the presence of both dG_6 and dA_8, the derived complex from *bm*-C*α*-PNA **1** exhibited the CD spectral profile (Figure 9c, trace **6C**) with positive bands around 220 and 263 nm

https://dx.doi.org/10.1021/acs.joc.0c02158
J. Org. Chem. XXXX, XXX, XXX−XXX

Table 2. ITC Binding of *bm*-Cα-PNA **1** to Complementary DNA **1** and DNA **2**[a]

entry	bimodal PNA/DNA	ΔG kcal/mol	ΔH kcal/mol	ΔS cal/mol·K	K_D M ($\times 10^{-6}$)	N
1	(*bm*-Cα-PNA **1**)$_2$:DNA **2** (triplex) **6A**	−8.52 ± 0.17	−28.4 ± 0.34	−69.0 ± 0.59	0.35 ± 0.05	0.5
2	*bm*-Cα-PNA **1**:DNA **1** (duplex) **5B**	−7.51 ± 0.23	−7.15 ± 0.28	−1.2 ± 0.8	2.0 ± 0.4	1.08
3	DNA **1**:*bm*-Cα-PNA **1**:DNA **2**:*bm*-Cα-PNA **1**:DNA **1** **6C** (double duplex of triplex)	−8.85 ± 0.43, −7.39 ± 0.38	−10.6 ± 2.23, −2.78 ± 0.47	−6.1 ± 1.5, +15.9 ± 1.3	0.2 ± 0.07, 2.51 ± 0.8	0.76, 1.28

[a]*N* = no. of nucleobase involved in binding from DNA/no. of nucleobase involved in binding from *bm*-Cα-PNA **1**.

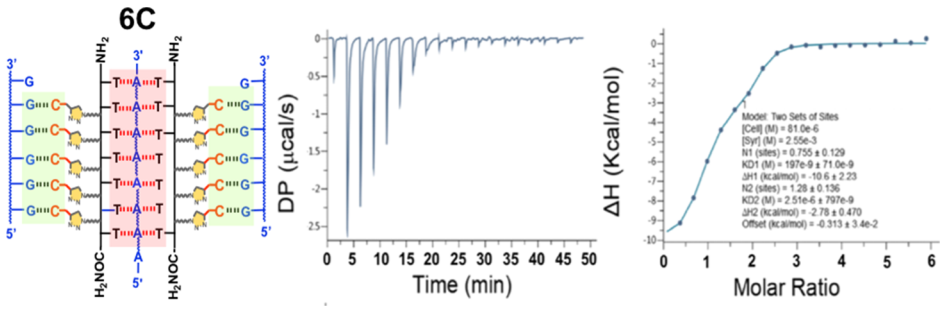

Figure 11. Bisignate ITC curves for association of double duplex of triplex **6C** from *bm*-Cα-PNA **1** with DNA **1** and DNA **2**

(shoulder at 228 nm) and a negative band at 245 nm. In comparison with t-amide triplex (Figure 9b, trace **6A**), the CD spectrum of the complex **6C** resembled the band profile around 220 nm but showed enhanced intensity of band at 260 nm, which is typical of duplex. The CD spectra of the complex **6C** is thus a composite of individual amide triplex (220 nm) and triazole duplex (260 nm), indicating the presence of both components in the complex leading to the formation of double duplex of triplex. Since the UV−*T* plot of this complex (Figure 6C) showed two transitions with enhanced T_ms, the observed CD is not a result of simple addition spectra of the individual triplex and duplex but arises from a composite complex of the double duplex of a triplex.

The mixed sequence bimodal PNA *bm*-Cα-PNA **2** in the presence of complementary dG_6 and DNA **3** forms a complex **6D** which shows a CD profile with a larger intensity positive band at 270 nm, minor band at 240 nm, and a positive tail beyond 220 nm (Figure 9c, trace **6D**). This profile is different from that seen for double duplex of triplex (Figure 9c, trace **6C**) and the isolated constituent t-amide (Figure 9b, trace **6B**) or triazole (Figure 9a trace **5C**) duplexes. This complex also shows two transitions in the UV−*T* plot with higher T_ms (Figure 6D) compared to individual duplexes, and the CD profile is similar to that of double duplex seen earlier for mixed sequence bimodal PNA.[12] Together, these results establish that *bm*-Cα-PNA **2** also form double duplex with DNA complementary to both t-amide and triazole faces.

Order of Formation of Double Duplex of Triplex. The double duplex of triplex (Figure 6C) can be assembled sequentially by two paths: path A involving first formation of triplex **6A**, followed by its duplex and path B with prior formation of duplex **5B** and then its triplex (Figure 10). Both pathways would lead to the same final composition of double duplex of triplex. This was assessed by following the CD spectral changes of *bm*-Cα-PNA **1** in path A by first adding dA_8 to produce the triplex **6A** (*bm*-Cα-PNA **1**)$_2$:dA_8 (Figure 10a, trace **6A**), followed by addition of dG_6 to generate the double duplex from triplex (Figure 10a, trace **6C**). In the second reaction by path B, the additions were reversed by first adding dG_6 to *bm*-Cα-PNA **1** to first prepare the duplex *bm*-Cα-PNA **1**:dG_6 (Figure 10b, trace **5B**), followed by addition of dA_8 to make the triplex of double duplex (Figure 10b, trace **6C**). The identity of intermediate triplex and duplex in each step could thus be recognized by their characteristic CD spectral profiles. It was seen that both experiments lead to the same final product with identical conformation, as seen by the overlapping CD profiles (Figure 10c). This experiment indicated that the paths used to reach the final product do not matter, and both sequences lead to same final assembly. Although the kinetics of the processes are not studied here, it appears that the assembly rates are fast enough to follow by CD and the experiment further confirms the formation of double duplex of a triplex from *bm*-Cα-PNA **1** in the presence of dA_8 and dG_6.

Thermodynamic Study of *bm*-Cα-PNA 1:DNA Complexes. The thermodynamic properties of the association of *bm*-Cα-PNA **1** with complementary DNA **1** (dG_6) and with DNA **2** (dA_8) were evaluated using isothermal titration calorimetry (ITC), to understand the driving forces for the formation of triazole duplex, t-amide triplex, and the double duplex of triplex. While the ITC experiment is straightforward for two-component binding systems, it is not easy to study sequential multicomponent binding events. The stepwise formation of individual duplex and triplex as studied by CD cannot be implemented by single ITC experiment to delineate thermodynamic parameters of each step. However, they can be obtained for the overall process by titrating *bm*-Cα-PNA **1** with an equimolar mixture of DNA **1** and DNA **2**. The concentration of each binding component was adjusted in terms of number of base pairs to enable determination of binding stoichiometry in terms of binding sites *N* (N_{DNA}/N_{PNA}, where N_{DNA} is total number nucleobases involved in binding from DNA and N_{PNA} is the number of nucleobases involved in binding from bimodal PNA). The various thermodynamic parameters enthalpy ΔH, entropy ΔS, dissociation constant K_D, and the stoichiometry of binding *N* obtained for different complexes from ITC experiments are shown in Table 2.

Binding Stoichiometry. The binding isotherm of *bm*-Cα-PNA **1** with dA_8 showed a nice sigmoidal profile (Supporting Information, Figures S17 and S18), suggesting the binding to be a cooperative process. The stoichiometry of binding was found to be 0.5 which corresponds to formation of triplex (*bm*-Cα-PNA **1**)$_2$:DNA **2** (dA_8), supporting the CD spectral result

https://dx.doi.org/10.1021/acs.joc.0c02158
J. Org. Chem. XXXX, XXX, XXX−XXX

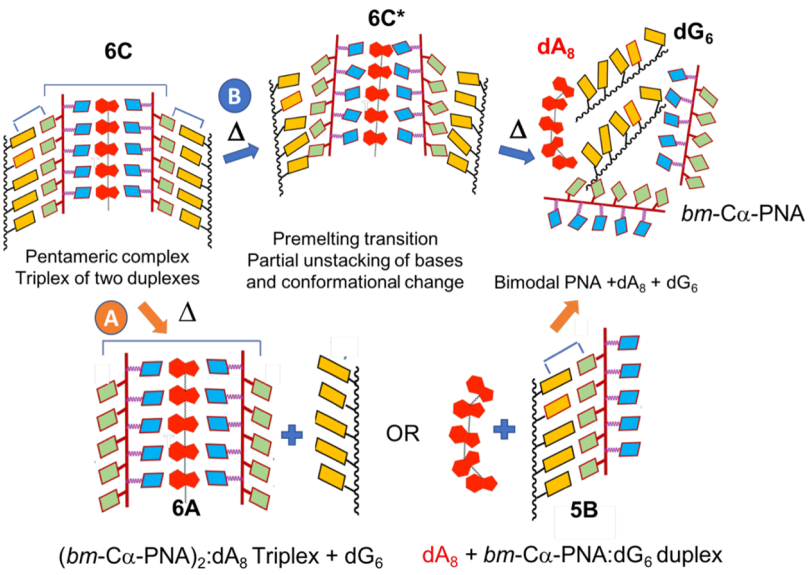

Figure 12. Cartoon model for melting pathways of pentameric double duplex of triplex. (A) Premelting transition followed by complete dissociation and (B) sequential melting via triplex/duplex intermediates.

(Figure 9b, **6A**). The binding of *bm*-C*α*-PNA **1** with DNA **1** (dG_6) similarly exhibited a sigmoidal profile with binding stoichiometry N corresponding to 1.08, indicating formation of 1:1 duplex as found from of Job's plot (Figure 4) and CD profile (Figure 9a, **5B**). When bimodal PNA *bm*-C*α*-PNA **1** was titrated with a mixture of DNA **1** and DNA **2**, by adjusting their concentration as per the number of base pairs, the binding isotherm was a double sigmoidal curve (two-step process) with the second transition distinctly seen at a molar ratio of 2. The ITC data could be fitted best to two sets of the binding site model (Figure 11).[22] Due to the partial overlapping of the two transitions, the number of binding components and two values of stoichiometry *N* 0.75 and 1.28 obtained are not easily interpretable as expected from stepwise binding.

Dissociation Constant K_D. The K_D for the triazole duplex *bm*-C*α*-PNA **1**:DNA **1** (**5B**) was around 2.0 ± 0.4 μM, while that for the triplex (*bm*-C*α*-PNA **1**)$_2$:DNA **2** **6A**) was 0.35 ± 0.05 μM, suggesting stronger binding of triplex compared to binding of duplex. For the double duplex of triplex (**6C**), the first binding ($K_{D1} \sim 0.2 \pm 0.07 \times 10^{-6}$ M) was about 10 times higher than the second binding ($K_{D2} \sim 2.51 \times 10^{-6}$ M). In comparison with K_D data on individual duplex/triplex, this may suggest that the first binding process is perhaps the triplex formation followed by double duplex, though such a sequential process is not conclusive, as discussed in section on UV−*T*.

Enthalpy, Entropy, and Free-Energy Factors. The enthalpy (ΔH) of formation of t-amide triplex (**6A**) (−28.4 kcal/mol) was about three times higher (more negative) than that of triazole duplex (**5B**) (−7.15 kcal/mol) in independent complexes. A similar trend is seen in bimodal PNA/DNA complex (**6C**) (−10.6 kcal/mol for the first transition and −2.78 kcal/mol for the second transition). The enthalpy of triplex in bimodal double duplex was three times lower (less negative) compared to that of the isolated complex. In terms of entropic factors, as expected, the termolecular t-amide triplex (*bm*-C*α*-PNA **1**)$_2$:dA_8 (**6A**) was less favored (more negative) compared to bimolecular triazole duplex (less negative). However, in double duplex of triplex (**6C**), the enthalpy is more negative and entropy is less negative (more positive), suggesting an enthalpic penalty for the entropic cost. This is reflected in the fact that the free energy for various complex formation are all in the range of −7.5 to −8.5 kcal/mol. Thus, the overall complex formation by bimodal PNA is a favorable process, driven by enthalpic factors which compensate for entropic losses. The ΔG and ΔH obtained here for various PNA/DNA complexes in bimodal PNA are similar to that reported earlier for unmodified PNA/DNA complexes.[23] It should be pointed out that the derived order of K_D values from ITC carried out at constant temperature cannot be directly correlated with T_m from UV−*T* experiments carried out at variable temperatures as they are measured under different conditions (isothermal vs variable temperature), and such a lack of agreement has precedence in the literature.[24]

Dissociation Model for Bimodal PNA/DNA Complexes. The double transitions observed in bimodal PNAs (Figure 6C) may arise either from sequential melting of triplex and duplex as in the case of DNA triplexes[20] or simultaneous dissociation of the composite complex as in PNA_2/DNA triplexes.[2,6] The simultaneous dissociation of the constituent strands in pentameric complex should give only one transition, and the occurrence of two transitions suggests that the melting is a two-step process, as shown in Figure 12. Path A involves sequential melting of the pentameric complex (**6C**) first of triplex and then of duplex (or reverse) into individual *bm*-C*α*-PNA **1** and DNA strands, but this does not explain the enhancement in T_m of each component. Once the triplex or duplex is formed after the first dissociation, further melting of each component is an independent process and should retain the T_m of isolated triplex/duplex. In the alternative path B, the complex (**6C**) may undergo a premelting transition to **6C**** comprising of conformational change with partial unwinding/unstacking of bases which are still held via H-bonding to give the first transition (T_{m1}). The large unstacking of bases in a tightly wound pentameric complex **6C*** would cause considerable absorbance increase conforming to the well-defined first transition. During the second step, this intermediate complex fully melts leading to complete disassociation yielding T_{m2}. The triplex/duplex in the complex (**6C**) are mutually coupled structurally since they are held

https://dx.doi.org/10.1021/acs.joc.0c02158
J. Org. Chem. XXXX, XXX, XXX−XXX

through the common bimodal PNA backbone. This also causes their melting to be coupled, stabilizing each other with enhancement of T_m in the complex. Though the exact mechanism and kinetics of dissociation cannot be deciphered from the present data, the observation of two transitions endorses that the bimodal PNAs bind from both sides to form higher order PNA/DNA complexes, which are more stable than the independent duplex/triplex components. A similar process accompanies the melting of the DNA **3**:*bm*-Cα-PNA **2**:dG_6 double duplex. The coexistence of duplex/triplex on *bm*-Cα-PNA **1**, and two duplexes on *bm*-Cα-PNA **2** with shared common PNA backbone causes synergistic enhancement in stability of constituent triplex and duplexes. In such systems, the initial melting of one duplex/triplex synchronously modulates the conformation of other duplex, thereby enhancing the T_ms of both components.

The premelting processes are well known in DNA duplexes[25] and involve cooperative perturbations in base stacking accompanied by non-cooperative changes in sugar-phosphate backbone conformation. In DNA−drug interactions, this may involve additional reorganization in spine of hydration. In the intermediate conformations adopted during premelting transitions termed premeltons,[25d] the bases are slightly unstacked but retain H-bonding with slight distortion. Premelting transitions are quite broad and ultimately lead to sharp transition with complete dissociation of both strands through breaking of H-bonds. They seem to be more prominent in higher order multicomponent assemblies from bimodal PNA described here that involve a greater number of base pairs. The role of additional stacking interactions by triazole rings is not clear at the moment. The proposed model needs further experimental investigation using selectively labeled DNA probes and computational studies.

CONCLUSIONS

The well-known standard *aeg*-PNA forms single duplex with cDNA (PNA/DNA) using nucleobases attached to the t-amide sidechain on the *aeg* backbone (t-amide duplex). The designed bimodal PNAs *bm*-Cα-PNA **1** and *bm*-Cα-PNA **2** described here have additional nucleobases conjugated at Cα in each repeating *aeg* unit and equipped to bind concurrently two complementary DNA sequences. The synthesis of bimodal PNA oligomers was achieved on the solid phase by sequential synthesis using Cα-ethylazido *aeg* PNA monomers (**1**−**4**) followed by a single-step click reaction to conjugate nucleobases on Cα-sidechain through a triazole linker. The *iso*-Cα-PNAs with nucleobases attached only at Cα-sidechain without t-amide linked nucleobases are new isomorphs of PNA. It is demonstrated that both *iso*-Cα-PNA and *bm*-Cα-PNA can bind to complementary DNA to form PNA/DNA duplexes from triazole face. The homo-oligomeric bimodal PNA *bm*-Cα-PNA **1** with T_7 sequence on t-amide side and C_5 on triazole side forms individual duplexes with dG_6 on triazole face and triplex with dA_8 from t-amide face. In the presence of both dA_8 and dG_6, the *bm*-Cα-PNA **1** yields a composite pentameric complex of double duplex (2× *bm*-Cα-PNA **1**:dG_6) of a triplex (*bm*-Cα-PNA **1**)$_2$:dA_8. This complex shows two transitions with T_ms higher than that of isolated complexes, which is indicative of synergistic stabilization of both duplex and triplex that coexist on a common PNA backbone. The ternary complex of *bm*-Cα-PNA **2** with a mixed sequence on t-amide side formed double duplex with two complementary DNAs.

The formation of triplex and duplexes from bimodal *bm*-Cα-PNA:DNA complexes is supported by characteristic CD spectral profiles. It was shown that the order of assembly of the pentameric complex by either triplex first and then its duplex or duplex first followed by triplex does not matter and leads to the same final complex. The ITC results of *bm*-Cα-PNA **1**:DNA binding indicated that the triazole duplex *bm*-Cα-PNA **1** had higher K_D with 6−10 times more favored dissociation than the amide face duplex. The unfavorable entropic barriers for bimodal PNA/DNA complexation is compensated by high enthalpic contributions arising from base stacking, possibly assisted by triazole stacks and H-bonding of complementary bases. The sequence specificity of base pairing of nucleobases on both triazole and amide faces was shown by lower T_ms of mismatched complexes. Together, these results provide proof of the design concept of bimodal PNA for simultaneously binding to complementary DNAs from both sides.

In *bm*-Cα-PNA **1** and *bm*-Cα-PNA **2** complexes with complementary DNAs, two duplexes or triplex and duplex coexist on a common bimodal PNA backbone that structurally couples both components, leading to their stabilization. The melting is not a sequential process and the two-step disassociation arises from a premelting conformational transition (T_{m1}) followed by simultaneous disassociation (T_{m2}) of both strands. The evidence for such a model of melting of double duplexes awaits further experiments with suitable designs of *bm*-Cα-PNAs to allow a systematic study of simultaneous binding and dissociation of coupled assemblies.

The bimodal PNAs described here and in the recent report[12] having nucleobases Cα/Cγ-sidechain demonstrate a new repertoire for generating higher order nucleic acid assemblies. Based on the choice of sequences on either side, bimodal PNAs can lead to construction of fused duplexes, triplexes, and tetraplexes (G_n/C_n) with complementary DNA and such elaboration is in progress in our laboratories. The derived supramolecular functional nanostructures will have potential applications in PNA material science.[26] The bimodal PNAs with hetero sequences on both faces may enable simultaneous targeting of two genes and micro RNA structures[27] for therapeutic purposes and PNA-based new gene editing methods.[3d,e] They may also serve to innovatively replace the short DNA staples for programmed folding of plasmids in DNA origami.[28]

EXPERIMENTAL SECTION

The chemicals used were of laboratory or analytical grade. All solvents used were distilled or dried to carry out different reactions. Reactions were monitored by thin layer chromatography (TLC). Usual workup involved sequential washing of the organic extract with water and brine followed by drying the organic layer over anhydrous sodium sulphate and evaporation of solvent under vacuum. TLCs were carried out on precoated silica gel GF_{254} sheets (Merck 5554). TLCs were analyzed under an UV lamp, iodine spray, and by spraying with ninhydrin solution, followed by heating of the plate. Column chromatographic separations were performed using silica gel (60−120 or 100−200 mesh). The syntheses of compounds **1**−**10** were carried out following the reported procedures described in the Supporting Information.[12a]

^{1}H and ^{13}C NMR spectra were recorded using Bruker AC-400 (400 MHz) or JEOL 400 MHz NMR spectrometers. The delta (δ) values for chemical shifts are reported in parts per million and are referred to internal standard TMS or deuterated NMR solvents. The optical rotation values were obtained on a Rudolph Research Analytical

https://dx.doi.org/10.1021/acs.joc.0c02158
J. Org. Chem. XXXX, XXX, XXX−XXX

Autopol V polarimeter. Mass spectra for reaction intermediates were obtained using Synapt G2 high definition mass spectrometry.

Solid Phase Synthesis of Bimodal Cα-PNA Oligomers. The synthesis of PNA oligomers was carried out using the solid phase synthesis protocol using the Boc strategy on MBHA (4-methylbenzhydryl amine) resin[16] with 0.20 mmol/g loading in a glass-sintered flask. The deprotection of the N-*t*-Boc group from the resin-bound lysine with 50% TFA in dichloromethane (DCM) (3 × 15 min) was followed by washing with DCM and dimethylformamide (DMF) (3 × 10 mL) to give a TFA salt of amine, which was neutralized using 10% DIPEA in DCM (3 × 10 min) to liberate free amine. After washing with DCM and DMF (3 × 10 mL), the free amine was coupled with carboxylic acid of the incoming monomers (**1**−**6**, 3 equiv) in DMF (500 μL) using HOBt (3 equiv), HBTU (3 equiv), and DIPEA (15 μL). After coupling reaction for 6 h, the reagents were removed by filtration and the resin was washed with DMF.

Solid Phase Click Reaction. After consecutive coupling of six units of monomer **1** (Scheme 2), the resin bound oligomer (10 mg resin, 0.20 mmol/g) having azido sidechain was subjected to the click reaction with nucleobase C-alkyne **9** (4.2 mg, 6 equiv) in the presence of CuI (12 mg, 18 equiv), ascorbic acid (3.0 mg, 5 equiv), and DIPEA (15 μL) in DMF:pyridine (1:1, v/v, 100 μL). The reaction was maintained for 5 min in the microwave at 65 °C and 25 W and then 24 h at room temperature. Excess reagents were removed by filtration, and the resin was washed with DMF, DCM, MeOH, and saturated EDTA. The *bm*-Cα-PNA **2** was synthesized similarly by stepwise coupling with desired monomers (**1**−**4**) followed by the click reaction at each step with appropriate nucleobase alkynes **9**.[12a]

Cleavage of the bm-Cα-PNA Oligomers from Solid Support. The MBHA resin (10 mg) after assembly of *bm*-Cα-PNA oligomers was stirred with thioanisole (20 μL) and 1,2-ethanedithiol (8 μL) in an ice bath for 10 min. TFA (200 μL) was added and cooled in an ice bath. TFMSA (16 μL) was added slowly with stirring, and the reaction mixture was stirred for 1.5−2 h at room temperature. The resin was removed by filtration under reduced pressure and washed twice with TFA, and the filtrate was evaporated on a rotary evaporator at ambient temperature. The filtrate was transferred to the microfuge tube, and the peptide was precipitated with cold diethyl ether. The peptide was isolated by centrifugation, and the precipitate was dissolved in 40% $MeNH_2$ solution to deprotect the isobutyl protecting group of nucleobases at rt for 8 h and again concentrated on speed vacuum, filtered, and purified by HPLC.

Purification of the PNA Oligomers by RP-HPLC. The purification of PNAs was carried out on a Dionex ICS 3000 HPLC system with semipreparative BEH130 C18 (10 × 250 mm) column using solvents water and acetonitrile with composition A: 0.1% TFA in CH_3CN/H_2O (5:95) and B = 0.1% TFA in CH_3CN/H_2O (1:1). The gradient for elution was 100% A to 100% B in 20 min, with a flow rate of 2 mL/min. The HPLC elutions were monitored at 220 and 254 nm wavelengths. The purity of oligomers was checked by reinjecting the sample on the C18 analytical column.

Characterization of the PNA Oligomers. MALDI-TOF mass spectrometry was used to confirm the integrity of the synthesized PNA oligomers using sinapinic acid (3,5-dimethoxy-4-hydroxycinnamic acid), 2,5-dihydroxybenzoic acid, or α-cyano-4-hydroxycinnamic acid as the matrix.

Temperature-UV Absorbance Measurements. UV-melting experiments were carried out on a Varian Cary 300 UV spectrophotometer equipped with a Peltier. The samples for T_m measurement were prepared by mixing the calculated amounts of respective oligonucleotides in the stoichiometric ratio (1:1, duplex) in sodium cacodylate buffer (10 mM) and NaCl (10 mM); pH 7.2 to achieve a final strand concentration of 3 μM for each strand. The samples were annealed by heating at 90 °C for 10 min followed by slow cooling to room temperature for at least 8−10 h and then refrigerated for at least 12−24 h. The samples (500 μL) were transferred to the quartz cell and equilibrated at the starting temperature for 5 min. The OD at 260 nm was recorded in steps from 20−92 °C with temperature increment of 0.5 °C. Each melting experiment was repeated at least twice. The normalized absorbance at 260 nm was plotted as a function of the temperature. The T_m was determined from the first derivative of normalized absorbance with respect to temperature and is accurate to ±1.0 °C. The data were processed using OriginPro 8.5, data were fitted by the sigmoidal curve, and the functions used were Boltzmann for one-face binding and biphasic dose response for two-face binding. The concentrations of all oligonucleotides were calculated on the basis of absorbance from the molar extinction coefficients of the corresponding nucleobases that is T = 8.8 $cm^2/\mu mol$; C = 6.6 $cm^2/\mu mol$; G = 11.7 $cm^2/\mu mol$; and A = 13.7 $cm^2/\mu mol$.[29]

CD Spectroscopy. CD spectra were recorded on a JASCO J-815 spectropolarimeter connected with a Peltier. The calculated amounts of PNA oligomers and the complementary DNA were mixed together in a stoichiometric ratio (1:1 for duplex) in sodium cacodylate buffer (10 mM) containing NaCl (10 mM); pH 7.2 to achieve a final strand concentration of 10 μM for each strand. The samples were annealed by heating at 90 °C for 10 min followed by slow cooling to room temperature for at least 8−10 h. The cooled samples were transferred to the refrigerator for at least 8−12 h. To record the CD spectra of PNA/DNA duplexes and single stranded PNAs, the temperature was maintained at 10 °C. The CD spectra were recorded as an accumulation of three scans from 300 to 190 nm using a 1 mm quartz cell, a resolution of 0.1 nm, bandwidth of 1 nm, sensitivity of 2 m deg, response of 1 s, and a scan speed of 50 nm/min.

ITC Study of Complexes of *bm*-Cα-PNA 1 with Complementary DNA. Thermodynamic properties of *bm*-Cα-PNA **1** complexation to cDNA were determined using ITC. The hybridization and binding studies of *bm*-Cα-PNA **1** with its complementary DNA oligonucleotides were carried out on Malvern MicroCal PEAQ ITC instrument. All titration experiments were performed at 15 °C in 10 mM sodium cacodylate buffer (pH 7.2) containing NaCl (10 mM). The buffer was used to prepare all solutions used in the experiment. The sample cell was loaded with *bm*-Cα-PNA **1** solution, and the reference cell contained only the buffer. The syringe was loaded with DNA solution (40 μL). The instrument was equilibrated at 15 °C until the baseline was flat and stable. The stirring speed was maintained at 700 rpm during the titrations.

Dilution experiments (DNA vs buffer) were performed at the same condition, and the measured heat of dilution was subtracted from the corresponding sample experiment. The binding isotherm was fitted to a "one set of binding sites" model for duplexes and triplexes. However, for double duplex of triplex, data best fitted in two sets of binding sites using MicroCal data analysis software to determine K_D, ΔG, ΔH, or $-\Delta S$ for all binding experiments. N corresponded to the ratio of number of nucleobases involved in binding from DNA and the number of nucleobases involved in binding from *bm*-Cα-PNA **1**.

■ ASSOCIATED CONTENT

Supporting Information

The Supporting Information is available free of charge at https://pubs.acs.org/doi/10.1021/acs.joc.0c02158.

Synthesis schemes and characterization data (NMR, MS of all new compounds, HPLC, MALDI-TOF of PNA oligomers, UV-melting curves, CD spectra, ITC data, and HRMS) (PDF)

■ AUTHOR INFORMATION

Corresponding Author

Krishna N. Ganesh − *Department of Chemistry, Indian Institute of Science Education and Research (IISER) Pune, Pune 411008, India; Department of Chemistry, Indian Institute of Science Education and Research (IISER) Tirupati, Tirupati 517507, India;* orcid.org/0000-0003-2292-643X; Email: kn.ganesh@iisertirupati.ac.in

https://dx.doi.org/10.1021/acs.joc.0c02158
J. Org. Chem. XXXX, XXX, XXX−XXX

Authors

Manoj Kumar Gupta − *Department of Chemistry, Indian Institute of Science Education and Research (IISER) Pune, Pune 411008, India; Department of Chemistry, Indian Institute of Science Education and Research (IISER) Tirupati, Tirupati 517507, India*

Bharath Raj Madhanagopal − *Department of Chemistry, Indian Institute of Science Education and Research (IISER) Tirupati, Tirupati 517507, India*

Complete contact information is available at: https://pubs.acs.org/10.1021/acs.joc.0c02158

Notes

The authors declare no competing financial interest.

■ ACKNOWLEDGMENTS

K.N.G. acknowledges Department of Science and Technology (DST), New Delhi for a research grant (EMR/2016/007601). M.K.G. thanks UGC, New Delhi for a research fellowship.

■ REFERENCES

(1) Egholm, M.; Buchardt, O.; Nielsen, P. E.; Berg, R. H. Peptide nucleic acids (PNA). oligonucleotide analogues with an achiral peptide backbone. *J. Am. Chem. Soc.* **1992**, *114*, 1895−1897.

(2) Nielsen, P.; Egholm, M.; Berg, R.; Buchardt, O. Sequence selective recognition of DNA by strand displacement with thymine substituted polyamide. *Science* **1991**, *254*, 1497−1500.

(3) (a) Nielsen, P. E. PNA technology. *Mol. Biotechnol.* **2004**, *26*, 233−248. (b) D'Agata, R.; Giuffrida, M. C.; Spoto, G. Peptide nucleic acid-based biosensors for cancer diagnosis. *Molecules* **2017**, *22*, 1951−1966. (c) Vilaivan, T. Fluorogenic PNA probes. *Beilstein J. Org. Chem.* **2018**, *14*, 253−281. (d) Saarbach, J.; Sabale, P. M.; Winssinger, N. Peptide nucleic acid (PNA) and its applications in chemical biology, diagnostics and therapeutics. *Curr. Opin. Chem. Biol.* **2019**, *52*, 112−124. (e) Economos, N. G.; Oyaghire, S.; Quijano, E.; Ricciardi, A. S.; Saltzman, W. M.; Glazer, P. M. Peptide nucleic acids and gene editing: Perspectives on structure and repair. *Molecules* **2020**, *25*, 735−736. (f) Canady, T. D.; Berlyoung, A. S.; Martinez, J. A.; Emanuelson, C.; Telmer, C. A.; Bruchez, M. P.; Armitage, B. A. Enhanced hybridization selectivity using structured gamma PNA probes. *Molecules* **2020**, *25*, 970−982.

(4) (a) Hyrup, B.; Egholm, M.; Nielsen, P. E.; Wittung, P.; Norden, B.; Buchardt, O. Structure-activity studies of the binding of modified peptide nucleic acids (PNAs) to DNA. *J. Am. Chem. Soc.* **1994**, *116*, 7964−7970. (b) Ganesh, K. N.; Nielsen, P. E. Peptide nucleic acids: Analogs and derivatives. *Curr. Org. Chem.* **2000**, *4*, 931−943. (c) Kumar, V. A.; Ganesh, K. N. Conformationally constrained PNA analogues: Structural evolution toward DNA/RNA binding selectivity. *Acc. Chem. Res.* **2005**, *38*, 404−412. (d) Govindaraju, T.; Kumar, V. A.; Ganesh, K. N. (SR/RS)-Cyclohexanyl PNAs: Conformationally preorganized PNA analogues with unprecedented preference for duplex formation with RNA. *J. Am. Chem. Soc.* **2005**, *127*, 4144−4145. (e) Corradini, R.; Sforza, S.; Tedeschi, T.; Totsingan, F.; Manicardi, A.; Marchelli, R. Peptide nucleic acids with a structurally biased backbone. Updated review and emerging challenges. *Curr. Top. Med. Chem.* **2011**, *11*, 1535−1554. (f) Moccia, M.; Adamo, M. F. A.; Saviano, M. Insights on chiral, backbone modified peptide nucleic acids: properties and biological activity. *Artif. DNA PNA XNA* **2014**, *5*, No. e1107176.

(5) (a) Dragulescu-Andrasi, A.; Rapireddy, S.; Frezza, B. M.; Gayathri, C.; Gil, R. R.; Ly, D. H. A simple gamma-backbone modification preorganizes peptide nucleic acid into a helical structure. *J. Am. Chem. Soc.* **2006**, *128*, 10258−10267. (b) Ishizuka, T.; Yoshida, J.; Yamamoto, Y.; Sumaoka, J.; Tedeschi, T.; Corradini, R.; Sforza, S.; Komiyama, M. Chiral introduction of positive charges to PNA for double-duplex invasion to versatile sequences. *Nucleic Acids Res.* **2008**, *36*, 1464−1471. Mitra, R.; Ganesh, K. N. PNAs grafted with (α/γ, R/S)-aminomethylene pendants: Regio and stereospecific effects on DNA binding and improved cell uptake. *Chem. Commun.* **2011**, *47*, 1198−1200. (d) Mitra, R.; Ganesh, K. N. Aminomethylene peptide nucleic acid (am-PNA): synthesis, regio-/ stereospecific DNA binding, and differential cell uptake of (α/γ, R/S) am-PNA analoguesr. *J. Org. Chem.* **2012**, *77*, 5696−5704. (e) Jain, D. R.; Anandi, L.; Lahiri, M.; Ganesh, K. N. Influence of pendant chiral Cγ-(alkylideneamino/guanidino) cationic side-chains of PNA backbone on hybridization with complementary DNA/RNA and cell permeability. *J. Org. Chem.* **2014**, *79*, 9567−9577.

(6) (a) Egholm, M.; Nielsen, P. E.; Buchardt, O.; Berg, R. H. Recognition of guanine and adenine in DNA by cytosine and thymine containing peptide nucleic acids (PNA). *J. Am. Chem. Soc.* **1992**, *114*, 9677−9678. (b) Egholm, M.; Buchardt, O.; Christensen, L.; Behrens, C.; Freier, S. M.; Driver, D. A.; Berg, R. H.; Kim, S. K.; Norden, B.; Nielsen, P. E. PNA hybridizes to complementary oligonucleotides obeying the Watson−Crick hydrogen-bonding rules. *Nature* **1993**, *365*, 566−568.

(7) (a) Brown, S.; Thomson, S.; Veal, J.; Davis, D. NMR solution structure of a peptide nucleic acid complexed with RNA. *Science* **1994**, *265*, 777−780. (b) Rasmussen, H.; Kastrup, J. S.; Nielsen, J. N.; Nielsen, J. M.; Nielsen, P. E. Crystal structure of a peptide nucleic acid (PNA) duplex at 1.7 A resolution. *Nat. Struct. Biol.* **1997**, *4*, 98−101. (c) Leijon, M.; Graeslund, A.; Nielsen, P. E.; Buchardt, O.; Norden, B.; Kristensen, S. M.; Eriksson, M. Structural characterization of PNA-DNA duplexes by NMR. Evidence for DNA in a B-like conformation. *Biochemistry* **1994**, *33*, 9820−9825. (d) Eriksson, M.; Nielsen, P. E. Solution structure of a peptide nucleic acid−DNA duplex. *Nat. Struct. Biol.* **1996**, *3*, 410−413. (e) Betts, L.; Josey, J. A.; Veal, J. M.; Jordan, S. R. A nucleic acid triple helix formed by a peptide nucleic acid-DNA complex. *Science* **1995**, *270*, 1838−1841.

(8) (a) Wojciechowski, F.; E. Hudson, R. Nucleobase modifications in peptide nucleic acids. *Curr. Top. Med. Chem.* **2007**, *7*, 667−679. (b) Sen, A.; Nielsen, P. E. Hydrogen bonding versus stacking stabilization by modified nucleobases incorporated in PNA·DNA duplexes Biophys. *Chem* **2009**, *141*, 29−33. (c) Endoh, T.; Annoni, C.; Hnedzko, D.; Rozners, E.; Sugimoto, N. Triplex-forming PNA modified with unnatural nucleobases: The role of protonation entropy in RNA binding. *Phys. Chem. Chem. Phys.* **2016**, *18*, 32002−32006. (d) Jayarathna, D. R.; Stout, H. D.; Achim, C. Metal coordination to ligand-modified peptide nucleic acid triplexes. *Inorg. Chem.* **2018**, *57*, 6865−6872.

(9) (a) Branda, N.; Kurz, G.; Lehn, J.-M. Janus wedges: A new approach towards nucleobase-pair recognition. *Chem. Commun.* **1996**, 2443−2444. (b) Chen, H.; Meena; McLaughlin, L. W. A Janus-wedge DNA triplex with A-W1-T and G-W2-C base triplets. *J. Am. Chem. Soc.* **2008**, *130*, 13190−13191. (c) Zhao, H.; Huang, W.; Wu, X.; Qing, Y.; Xing, Z.; He, Y. Synthesis of a complete Janus-type guanosine-cytosine base and its 2'-deoxyribonucleoside. *Chem. Lett.* **2011**, *40*, 684−686. (d) Shin, D.; Tor, Y. Bifacial nucleoside as a surrogate for both T and A in duplex DNA. *J. Am. Chem. Soc.* **2011**, *133*, 6926−6929. (e) Artigas, G.; Marchán, V. Synthesis of Janus compounds for the recognition of G-U mismatched nucleobase pairs. *J. Org. Chem.* **2013**, *78*, 10666−10677.

(10) (a) Xia, X.; Piao, X.; Bong, D. Bifacial peptide nucleic acid as an allosteric switch for aptamer and ribozyme function. *J. Am. Chem. Soc.* **2014**, *136*, 7265−7268. (b) Thadke, S. A.; Hridya, V. M.; Perera, J. D. R.; Gil, R. R.; Mukherjee, A.; Ly, D. H. Shape selective bifacial recognition of double helical DNA. *Comm. Chem.* **2018**, *1*, 79. (c) Thadke, S. A.; Perera, J. D. R.; Hridya, V. M.; Bhatt, K.; Shaikh, A. Y.; Hsieh, W.-C.; Chen, M.; Gayathri, C.; Gil, R. R.; Rule, G. S.; Mukherjee, A.; Thornton, C. A.; Ly, D. H. Design of bivalent nucleic acid ligands for recognition of RNA-repeated expansion associated with Huntington's disease. *Biochemistry* **2018**, *57*, 2094−2108.

(11) (a) Madsen, C. S.; Nielsen, L. J.; Pedersen, N. S.; Lauritsen, A.; Nielsen, P. Double-headed nucleotides in DNA-zipper structures; base-base interactions and UV-induced cross-coupling in the minor groove. *RSC Adv.* **2013**, *3*, 10696−10706. (b) Kumar, P.; Sharma, P.

K.; Nielsen, P. Double-headed nucleotides with arabino configuration: Synthesis and hybridization properties. *J. Org. Chem.* **2014**, *79*, 11534−11540. (c) Dalager, M.; Andersen, N. K.; Kumar, P.; Nielsen, P.; Sharma, P. K. Double-headed nucleotides introducing thymine nucleobases in the major groove of nucleic acid duplexes. *Org. Biomol. Chem.* **2015**, *13*, 7040−7049. (d) Sharma, P. K.; Kumar, P.; Nielsen, P. Double-headed nucleotides: Building blocks for new nucleic acid architectures. *Aust. J. Chem.* **2016**, *69*, 1094−1101. (e) Hornum, M.; Stendevad, J.; Sharma, P. K.; Kumar, P.; Nielsen, R. B.; Petersen, M.; Nielsen, P. Base-pairing properties of double-headed nucleotides. *Chem.—Eur. J.* **2019**, *25*, 7387−7395. (f) Kumar, P.; Sorinas, A. F.; Nielsen, L. J.; Slot, M.; Skytte, K.; Nielsen, A. S.; Jensen, M. D.; Sharma, P. K.; Vester, B.; Petersen, M.; Nielsen, P. Double-coding nucleic acids: Introduction of a nucleobase sequence in the major groove of the dna duplex using double-headed nucleotides. *J. Org. Chem.* **2014**, *79*, 8020−8030. (g) Umemoto, T.; Wengel, J.; Madsen, A. S. Functionalization of 2′-amino-LNA with additional nucleobases. *Org. Biomol. Chem.* **2009**, *7*, 1793−1797.

(12) (a) Gupta, M. K.; Madhanagopal, B. R.; Datta, D.; Ganesh, K. N. Structural design and synthesis of bimodal PNA that simultaneously binds two complementary DNAs to form fused double duplexes. *Org. Lett.* **2020**, *22*, 5255−5260. (b) Bhingardeve, P.; Madhanagopal, B. R.; Ganesh, K. N. Cγ(S/R)-Bimodal peptide nucleic acids (Cγ-bm-PNA) synchronously bind two different cDNA strands to form coupled double duplexes with enhanced stability. *J. Org. Chem.* **2020**, *85*, 13680−13693.

(13) (a) Rippe, K.; Ramsing, N. B.; Klement, R.; Jovin, T. M. A parallel stranded linear DNA duplex incorporating dG·dC base pairs. *J. Biomol. Struct. Dyn.* **1990**, *7*, 1199−1209. (b) Szabat, M.; Kierzek, R. Parallel-stranded DNA and RNA duplexes − structural features and potential applications. *FEBS J.* **2017**, *284*, 3986−3998.

(14) Dueholm, K. L.; Petersen, K. H.; Jensen, D. K.; Egholm, M.; Nielsen, P. E.; Buchardt, O. Peptide nucleic acid (PNA) with a chiral backbone based on alanine. *Bioorg. Med. Chem. Lett.* **1994**, *4*, 1077−1080.

(15) (a) Porcheddu, A.; Giacomelli, G.; Piredda, I.; Carta, M.; Nieddu, G. A Practical and efficient approach to PNA monomers compatible with fmoc-mediated solid-phase synthesis protocols. *Eur. J. Org. Chem.* **2008**, 5786−5797. (b) Kramer, R. A.; Bleicher, K. H.; Wennemers, H. Design and synthesis of nucleoproline amino acids for the straightforward preparation of chiral and conformationally constrained nucleopeptides. *Helv. Chim. Acta* **2012**, *95*, 2621−2634. (c) Nagapradeep, N.; Verma, S. Characterization of an unprecedented organomercury adduct via Hg(ii)-mediated cyclization of N9-propargylguanine. *Chem. Commun.* **2011**, *47*, 1755−1757.

(16) *Peptide Nucleic Acids Protocols and Applications*, 2nd ed.; Nielsen, P. E., Ed.; Horizon Bioscience: Norfolk, U.K., 2004.

(17) (a) Bentin, T.; Hansen, G. I.; Nielsen, P. E. Measurement of PNA binding to double-stranded DNA. *Methods in Molecular Biology*; Nielsen, P. E., Ed.; Humana Press: Totowa, NJ, 2002; Vol. *208*, pp 91−109. (b) Jasiński, M.; Miszkiewicz, J.; Feig, M.; Trylska, J. Thermal stability of peptide nucleic acid complexes. *J. Phys. Chem. B* **2019**, *123*, 8168−8177.

(18) (a) Job, P. Formation and stability of inorganic complexes in solution. *Ann. Chim.* **1928**, *9*, 113−203. (b) Huang, C. Y. Determination of binding stoichiometry by the continuous variation method: the Job plot. *Methods Enzymol.* **1982**, *87*, 509−525.

(19) (a) Puglisi, J. D.; Tinoco, I., Jr. Absorbance melting curves of RNA. *Methods Enzymol.* **1989**, *180*, 304−325. (b) Mergny, J.-L.; Lacroix, L. Analysis of thermal melting curves. *Oligonucleotides* **2003**, *13*, 515−537.

(20) Plum, G. E.; Park, Y. W.; Singleton, S. F.; Dervan, P. B.; Breslauer, K. J. Thermodynamic characterization of the stability and the melting behavior of a DNA triplex: A spectroscopic and calorimetric study. *Proc. Natl. Acad. Sci. U.S.A.* **1990**, *87*, 9436−9440.

(21) Corradini, R.; Tedeschi, T.; Sforza, S.; Marchelli, R. Electronic circular dichroism of peptide nucleic acids and their analogues. In *Comprehensive Chiroptical Spectroscopy: Applications in Stereochemical Analysis of Synthetic Compounds, Natural Products, and Biomolecules*; Berova, N.; Polavarapu, P. L., Nakanishi, K., Woody, R. W., Eds.; John Wiley & Sons, Inc., 2012; Vol. 2, pp 581−617.

(22) Bartold, K.; Pietrzyk-Le, A.; Golebiewska, K.; Lisowski, W.; Cauteruccio, S.; Licandro, E.; D'Souza, F.; Kutner, W. Oligonucleotide determination via peptide nucleic acid macromolecular imprinting in an electropolymerized CG-Rich artificial oligomer analogue. *ACS Appl. Mater. Interfaces* **2018**, *10*, 27562−27569.

(23) (a) Ratilainen, T.; Holmén, A.; Tuite, E.; Nielsen, P. E.; Nordén, B. Thermodynamics of sequence-specific binding of PNA to DNA. *Biochemistry* **2000**, *39*, 7781−7791. (b) Krupnik, O. V.; Guscho, Y. A.; Sluchanko, K. A.; Nielsen, P. E.; Lazurkin, Y. S. Thermodynamics of the melting of PNA_2/DNA triple helices. *J. Biomol. Struct. Dyn.* **2001**, *19*, 535−542.

(24) (a) Schwarz, F.; Robinson, S.; Butler, J. M. Thermodynamic comparison of PNA/DNA and DNA/DNA hybridization reactions at ambient temperature. *Nucleic Acids Res.* **1999**, *27*, 4792−4800. (b) Chakrabarti, M.; Schwarz, F. P. Thermal stability of PNA/DNA and DNA/DNA duplexes by differential scanning calorimetry. *Nucleic Acids Res.* **1999**, *27*, 4801−4806.

(25) (a) Xu, D.; Evans, K. O.; Nordlund, T. M. Melting and premelting transitions of an oligomer measured by DNA base fluorescence and absorption. *Biochemistry* **1994**, *33*, 9592−9599. (b) Chen, Y. Z.; Prohofsky, E. W. Differences in melting behaviour between homopolymers and copolymers of DNA: Role of nonbonded forces for GC and the role of the hydration spine and pre-melting transition for AT. *Biopolymers* **1993**, *33*, 797−812. (c) Movileanu, L.; Benevides, J. M.; Thomas, G. J., Jr. Determination of base and backbone contributions to the thermodynamics of premelting and melting transitions in B DNA. *Nucleic Acids Res.* **2002**, *30*, 3767−3777. (d) Sobell, H. M. Premeltons in DNA. *J. Struct. Funct. Genomics* **2016**, *17*, 17−31.

(26) (a) Manicardi, A.; Rozzi, A.; Korom, S.; Corradini, R. Building on the peptide nucleic acid (PNA) scaffold: a biomolecular engineering approach. *Supramol. Chem.* **2017**, *29*, 784−795. (b) Duan, T.; He, L.; Tokura, Y.; Liu, X.; Wu, Y.; Shi, Z. Construction of tunable peptide nucleic acid junctions. *Chem. Commun.* **2018**, *54*, 2846−2849. (c) Swenson, C. S.; Velusamy, A.; Argueta-Gonzalez, H. S.; Heemstra, J. M. Bilingual peptide nucleic acids: Encoding the languages of nucleic acids and proteins in a single self-assembling biopolymer. *J. Am. Chem. Soc.* **2019**, *141*, 19038−19047.

(27) Cadoni, E.; Manicardi, A.; Madder, A. PNA-based microRNA detection methodologies. *Molecules* **2020**, *25*, 1296−1321.

(28) (a) Hong, F.; Zhang, F.; Liu, Y.; Yan, H. DNA origami: Scaffolds for creating higher order structures. *Chem. Rev.* **2017**, *117*, 12584−12640. (b) Bila, H.; Kurisinkal, E. E.; Bastings, M. M. C. Engineering a stable future for DNA-origami as a biomaterial. *Biomater. Sci.* **2019**, *7*, 532−541.

(29) Sahu, B.; Sacui, I.; Rapireddy, S.; Zanotti, K. J.; Bahal, R.; Armitage, B. A.; Ly, D. H. Synthesis and characterization of conformationally preorganized, (R)-diethylene glycol-containing γ-peptide nucleic acids with superior hybridization properties and water solubility. *J. Org. Chem.* **2011**, *76*, 5614−5627.

https://dx.doi.org/10.1021/acs.joc.0c02158
J. Org. Chem. XXXX, XXX, XXX−XXX